Can we retrieve a paleoclimatic signal from the deeper part of the EPICA Dome C ice core?

Jean-Louis Tison[a], Martine de Angelis[b], Geneviève Littot[c], Eric Wolff[c], Hubertus Fischer[d], Margareta Hansson[e], Matthias Bigler[d], Roberto Udisti[f], Anna Wegner[g], Jean Jouzel[h], Barbara Stenni[i], †Sigfus Johnsen[j], Valérie Masson-Delmotte[h], Amaëlle Landais[h], Volodya Lipenkov[k], Laetitia Loulergue[b], †Jean-Marc Barnola[b], Jean-Robert Petit[b], Barbara Delmonte[l], Gabrielle Dreyfus[m], Dorthe Dahl-Jensen[j] ,Gael Durand[b], Bernhard Bereiter [d], Adrian Schilt[d], Renato Spahni[d], K. Pol[c], Réginald Lorrain[a] ,Roland Souchez[a] and Denis Samyn[n]

[a] Laboratoire de Glaciologie, Université Libre de Bruxelles, CP 160/03, 50, av. F.D. Roosevelt, 1050-Bruxelles, Belgium

[b] Laboratoire de Glaciologie et Géophysique de l'Environnement, 54, rue Molière Domaine Universitaire 38402 Saint-Martin d'Hères, France

[c] British Antarctic Survey, High Cross, Madingley Road, Cambridge CB3 OET, United Kingdom

[d] Climate and Environmental Physics, Physics Institute & Oeschger Centre for Climate Change Research, University of Bern, Sidlerstrasse 5, 3012 Bern, Switzerland.

[e] Department of Physical Geography and Quaternary Geology, Stockholm University, S-106 91 Stockholm, Sweden.

[f.] University of Florence. Chemistry Dept., via della Lastruccia, 3 – 50019 Sesto Fiorentino (Florence), Italy.- udisti@unifi.it

Can we retrieve a clear paleoclimatic signal from the deeper part of the EPICA Dome C ice core?

[g]Alfred Wegener Institute, Bremerhaven, Germany

[h] Laboratoire des Sciences du Climat et de l'Environnement/Institut Pierre Simon Laplace, CEA-CNRS-UVSQ, CEA Saclay, 91191, Gif-sur -Yvette, France

[i] Dipartimento di Scienze Ambientali, Informatica e Statistica, Università Ca' Foscari, Venezia, Italy

[j] Niels Bohr Institute, Juliane Maries Vej 30, 2100 Copenhagen, Denmark

[k] Arctic and Antarctic Research Institute, 38 Bering str., St.Petersburg, Russia

[l] DISAT, Dept. of Earth and Environmental Sciences, University Milano Bicocca, Piazza della Scienza 1, 20126 Milano, Italy.

[m] Office of Policy and International Affairs, U.S. Department of Energy, Washington, DC 20585

[n] Nagaoka University of Technology, 1603-1 Kamitomioka, Nagaoka, Niigata 940-2188 Japan

*Corresponding author :

Tison, Jean-Louis

Laboratoire de Glaciologie

Faculté des Sciences - CP 160/03

Université Libre de Bruxelles

50, avenue F.D. Roosevelt,

1050 - Bruxelles

jtison@ulb.ac.be

Tel: +32 2 650 22 25

Fax: +32 2 650 22 26

Formatted: French (Belgium)

Abstract

An important share of paleoclimatic information is buried within the lowermost layers of deep ice cores. Because improving our records further back in time is one of the main challenges in the near future, it is essential to judge how deep these records remain unaltered, since the proximity of the bedrock is likely to interfere both with the recorded temporal sequence and the ice properties. In this paper, we present a multiparametric study (δD-$\delta^{18}O_{ice}$, $\delta^{18}O_{atm}$, total air content, CO_2, CH_4, N_2O, dust, high resolution chemistry, ice texture) of the bottom 60 meters of the EPICA Dome C ice core from central Antarctica. These bottom layers were subdivided in two distinct facies: the lower 12 meters showing visible solid inclusions (basal dispersed ice facies) and the 48 meters above, which we will refer to as the "basal clean ice facies". Some of the data are consistent with a pristine paleoclimatic signal, others show clear anomalies. It is demonstrated that neither large scale bottom refreezing of subglacial water, nor mixing (be it internal or with a local basal end-term from a previous/initial ice sheet configuration) can explain the observed bottom ice properties. We focus on the high-resolution chemical profiles and on the available remote sensing data on the subglacial topography of the site to propose a mechanism by which relative stretching of the bottom ice sheet layers is made possible, due to the progressively confining effect of subglacial valley sides. This stress field change, combined with bottom ice temperature close to the pressure melting point, induces accelerated migration recrystallization, which results in spatial chemical sorting of the impurities, depending on their state (dissolved vs. solid) and if they are involved or not in salt formation. This chemical sorting effect is responsible for the progressive build-up of the visible solid aggregates

that therefore mainly originate “from within”, and not from incorporation processes of debris from the ice sheet’s substrate. We further discuss how the proposed mechanism is compatible with the other ice properties described. We conclude that the paleoclimatic signal is only marginally affected in terms of global ice properties at the bottom of EPICA Dome C, but that the time scale was considerably distorted by mechanical stretching of MIS20 due to the increasing influence of the subglacial topography, a process that might have started well above the bottom ice. A clear paleoclimatic signal can therefore not be inferred from the deeper part of the EPICA Dome C ice core. Our work suggests that the existence of a flat monotonic ice-bedrock interface, extending for several times the ice thickness, would be a crucial factor in choosing a future “oldest ice” drilling location in Antarctica.

Keywords

Antarctica; EPICA Dome C; ice core; Bottom ice; Paleoclimate; Multiparametric analyses

1. Introduction: Paleoclimatic signals in basal layers of deep ice cores

Deep ice cores retrieved from the two present-day major ice sheets on Earth, Greenland in the North and Antarctica in the South, delivered a wealth of unique paleoclimatic archives over the last decades. These allowed reconstruction of global climatic and environmental conditions over the last 800.000 years, including unprecedented records of cyclic changes in the composition of greenhouse gases (CO_2, CH_4, N_2O). An important share of those paleoclimatic information is buried within the lowermost sections of those deep ice cores, due to the mechanical thinning of annual accumulation layers with depth. Improving the records further back in time is therefore one of the main challenges of ice core science in the near future (IPICS, 2009). A major concern in this regard is to judge how far down we can trust the paleoclimatic signals stored within the ice, since the proximity of the bedrock is likely to interfere both with the recorded temporal sequence and with the ice properties. This in turn is closely linked to the thermal and hydrological regime at the bottom of the ice sheet, as shown previously in the literature describing basal layers of deep ice cores (e.g. Goodwin, 1993, Gow et al., 1979, Gow and Meese, 1996, Herron and Langway, 1979, Jouzel et al., 1999, Koerner and Fisher, 1979, Souchez, 1997, Souchez et al., 1998, Souchez et al., 1995a, Souchez et al., 2006, Souchez et al., 1995b, Souchez et al., 1993b, Souchez et al., 2003, Souchez et al., 2002b, Souchez et al., 2000a, Souchez et al., 1994, Tison et al., 1998, Tison et al., 1994, Weis et al., 1997). In some cases, where the ice-bedrock interface is clearly below the pressure-melting point (pmp) as, for example, at the GRIP (-9°C) or the Dye-3 (-12°C) ice coring sites in Greenland, single or multiple mixing events between the present-day ice sheet ice and local ice remnants of previous (or

even initial) ice sheet configurations are encountered (Souchez, 1997, Souchez et al., 1998, Souchez et al., 1994, Souchez et al., 2000b, Verbeke et al., 2002). Where the ice-bedrock interface is at the pmp, the meteoric ice has the potential to melt at a rate that will depend on the heat budget at the ice-bedrock interface (geothermal heat flux, internal friction and conduction through the overlying ice). In some cases, where the subglacial topography allows it, like at the Antarctic Vostok site, a subglacial lake will exist. Again, depending on the heat budget but also on the subglacial lake water circulation pattern, lake ice will form at the ice-water interface in substantial amounts (e.g. Jouzel et al., 1999, Souchez et al., 2002a, Souchez et al., 2003, Souchez et al., 2000a). This ice, evidently, does not carry paleoclimatic information. Furthermore, in the case of large subglacial lakes (such as Lake Vostok) where the ice column above can be considered in full hydrostatic equilibrium buoyancy, re-grounding of the ice sheet on the lee side of the lake will induce dynamical perturbations (such as folds), even in the meteoric ice above, as demonstrated for MIS11 (Raynaud D., 2005) and for the ice just above the accreted lake ice (Souchez et al., 2002a, Souchez et al., 2003, Souchez et al., 2002b). A less well documented case however, is the one where no significant water body exists at the ice-bedrock interface. If only melting occurs at the interface, with no water accumulation and no refreezing (as, for example at the NGRIP site in Greenland), can we then rely on the paleoclimatic information gathered in the basal layers? The EPICA Dome C ice core potentially provides us with an opportunity to investigate that specific case. In this paper, we are using a multiparametric approach, combining new and existing low resolution (50cm) data for the bottom 60 meters of ice from the EDC ice core with a new high resolution (1.5 to 8 cm) chemical data set in order to better

understand the processes at work and evaluate how these might have altered the environmental archive.

2. The EPICA Dome C ice core

The Dome C deep ice core (EDC) is one of the two ice cores drilled in the framework of the European Project for Ice Coring in Antarctica (EPICA). It is located at Concordia Station (Dome C - 75°06'04"S; 123°20'52" E), about 1200 km south of the French coastal station of Dumont d'Urville, and 720 km north east of the Russian Vostok Station. Detailed GPS surface topography and airborne radar surveys were conducted in 1994-1995 in order to optimize the choice for the drilling location (Rémy and Tabacco, 2000; Tabacco et al., 1998). These provided clear features of the bedrock and surface topography, showing a set of north-south-trending parallel valleys around 20 km wide and 200-400 meters deep in the bedrock, corresponding to smooth elongated undulations a few meters high at the surface.

A final drilling depth of 3259.72m was reached in December 2004, about 15 meters above the ice-bedrock interface (to prevent from eventually making contact with subglacial meltwaters). The ice temperature was -3°C at 3235m and a simple extrapolation to the bottom indicates that the melting point should be reached at the interface (Lefebvre et al., 2008). The top ca. 3200m of the EDC ice core have already been extensively studied and provided a full suite of climatic and environmental data over the last 8 climatic cycles (e.g. Delmonte et al., 2008, Durand et al., 2008, EPICA Community members, 2004, Jouzel et al., 2007, Lambert et al., 2008, Loulergue et al., 2008, Lüthi et al., 2008, Wolff et al., 2006). Raisbeck et al. (2006) confirmed the old age

of the deep EDC ice by presenting evidence for enhanced ^{10}Be deposition in the ice at 3160-3170m (corresponding to the 775-786 kyr interval in the EDC2 time scale) consistent with the age and duration of the Matuyama-Brunhes geomagnetic reversal. A coherent interpretation of CO_2 and CH_4 profiles (Lüthi et al., 2008, Loulergue et al., 2008) also established the presence of Marine Ice Stages (MIS) 18 (ca. 739-767 kyr BP) and 19 (ca. 767-790 kyr BP). However, a detailed study of the isotopic composition of O_2 and its relationship to daily northern hemisphere summer insolation and comparison to marine sediment records showed potentially anomalous flow in the lowermost 500m of the core with associated distortion of the EDC2 time scale by a factor of up to 2. This led to the construction of the new, currently used, EDC3 timescale (Parrenin et al., 2007). Note that efforts are still ongoing to refine this timescale, combining multi-site data sets and using $\delta^{18}O_{atm}$ and O_2/N_2 as proxies for orbital tuning (Landais et al., 2012; Bazin et al., 2013).

As described below, the bottom 60 meters of the available core acquired distinctive properties, as a result of processes driven by the proximity of the ice-bedrock interface. We will therefore, in accordance with the previous literature (e.g. Knight, 1077; Hubbard et al., 2009) refer to it as “basal ice”. The last 12 meters of the available core show visible solid inclusions (Fig. 1a), which are traditionally interpreted as a sign of interactions with the bedrock. These inclusions are spherical in shape, brownish to reddish in color, and generally increase both in size and density with increasing depth. They however remain evenly distributed within the ice, therefore qualifying as a “basal dispersed facies” in existing classifications (e.g. Hubbard et al., 2007). Between 3248.30 m (first occurrence of inclusion visible by eye) and 3252.15m the inclusions are

only sparse (0 to 10 inclusions per 55 cm ice core length) and less than 1mm in diameter. In the lower 8 meters, inclusions get bigger (up to 3 mm in the last 50 cm sample) and reach more than 20 individual inclusions per 50 cm ice core length. In several cases, especially for the bigger inclusions, these are “enclosed” in a whitish ovoid bubble-like feature (e.g. upper left corner of Fig. 1a). Careful visual examination of the texture of each individual inclusion suggests that these generally consist of a large number of smaller aggregates although individual particles also occur. In most cases, these inclusions appear to be located at crystal boundaries. A detailed study of the morphology, mineralogy and chemistry of some of these individual inclusions is described elsewhere (de Angelis et al.,2013). Finally, it should be kept in mind that these characteristics are valid for ice collected between 6 and 15 meters above the actual ice-bedrock interface. We do not, unfortunately, have any information on the properties of the ice below, the thickness of which was estimated using a downhole seismometer (J. Schwander, pers. comm., 2011). The upper 48 meters of the basal ice sequence will be referred to as the “basal clean ice facies” (i.e. devoid of visible inclusions), also in line with previous work (Hubbard et al., 2007).

3. Material and Methods

The dispersed facies of the basal ice of the EDC core shows a relatively low debris content, compared to the other deep ice coring sites described in previous studies (Camp Century, GRIP, Dye-3, Vostok), and could therefore be processed in continuity with the cutting scheme used for the EDC ice above. The multi-parametric data set discussed in this paper was therefore obtained applying analytical techniques described

in full in previous studies focusing on single parameters. We are summarizing those in the "supplementary material", referring to the appropriate previous literature for full details.

4. The basal ice properties: a multiparametric approach

Figure 1 b and c plot the full δD profile of the EPICA ice core, vs. depth and age respectively (EDC3 time scale, Parrenin et al., 2007). As stated above, we will use the "dispersed ice facies" terminology for the lower 12 meters (red open triangles) and qualify the 48 meters above as the "clean ice facies" (blue open squares); "basal ice" will refer to the whole 60 meters sequence. A combined Vostok-EDC $\delta^{18}O_{atm}$ profile (isotopic composition of atmospheric oxygen in ice) vs. EDC3 time scale is shown in Figure 1d (adapted from Dreyfus et al., 2007, Petit et al., 1999 for the ice above 3200m). The δ^{18}O benthic record stack of Lisiecki and Raymo (2005) is also plotted as a reference in Figure 1e. The co-isotopic properties of the EPICA Dome C bottom ice (open squares for clean ice facies, open triangles for dispersed ice facies) are described in Figure 2a (δD vs. δ^{18}O) and 2b (d_{excess} vs. δD) and compared to those of the ice from the last 140 ky (Stenni et al., 2010). Work in progress on the co-isotopic properties of the older ice (down to 3189.45m) shows that the latter do not differ from the trends seen in Figure 2 (B. Stenni et al., unpublished data).

Figure 3 and Table S1 summarize the available low resolution gas and insoluble dust concentrations data. CH_4, CO_2 and N_2O are covered for both the clean (squares in Fig. 3a) and dispersed (triangles in Fig. 3a) facies while total gas content (grey dots in Fig. 3a) is only available for the clean ice facies. The full concentrations ranges observed for

CH_4 (Loulergue et al., 2008),CO_2 (Lüthi et al., 2008), N_2O (Schilt et al. 2010) and total gas content (Raynaud et al., 2007) during the preceding climatic cycles are also shown for reference, as white, black, light grey and dark grey vertical bars respectively. The limited number of dust concentration measurements available is shown in Figure 3b (same symbols as above) and also compared to the full range of values observed during the previous climatic cycles (black vertical bar, Delmonte et al., 2008)).

Clean and dispersed basal ice facies concentrations of selected chemical species (MSA, SO_4, Ca, Mg, Na, K, Cl, NO_3) are presented in two complementary ways, in Figures 4 and 5. In Figure 4 high-resolution (1.5 to 5 cm) profiles of discrete sections in the clean (open squares) and dispersed (open triangles) facies are shown, along with the 5-8 cm resolution profile in the ice above 3200m (black dots, courtesy of the EPICA Chemistry Consortium). In Figure 5, the same data set is re-arranged as a simple frequency distribution within bins of 5 or 1 ngg^{-1} depending on the species. Clean facies is plotted as open squares on thick solid line and dispersed facies as open triangles on thick dotted line. All data from preceding "full glacial" intervals (i.e. excluding interglacials and complete transitions) are plotted as a background in thin grey lines with incremented symbols (see caption in upper left graph for MSA). Table 1 summarizes the data set used in Figure 5 in terms of concentration means and 1σ values, with the depth and isotopic ranges associated to each time interval chosen. The "full glacial" intervals were selected on careful analysis of the δD data set, keeping for each glacial period the samples with the lowest values and using the location of increasing isotopic gradient with depth as a cutting point on both sides. We discuss in the supplementary material section why we believe we can compare the results from these various groups of

samples shown in Figure 5 and Table 1, despite the fact that they cover different time windows.

Finally, Figure 6 plots the mean equivalent crystal radii for the deep and basal ice, as obtained from preliminary measurements in the field, and compare those to measurements using Automatic Ice Texture Analyzers as described in Durand et al. (2009). Reliable measurement of crystals radii in the bottom ice using automatic techniques is hampered by the very large increase of crystal sizes, often spanning several individual thin sections. Only "unconventional" measurements such as e.g. sonic logging (still in development) might allow us to document these properties further in the future.

5. Discussion

5.1. Indicators of an "undisturbed" paleoclimatic record

In this first section of the discussion, we will demonstrate that some of the clean and dispersed basal ice facies properties appear coherent with a climatic signature unmodified by large scale refreezing processes. As shown in Figure 1b,c both the clean and dispersed ice facies display δD values typical of a mild to cold glacial period, with respective ranges of -427.7 to -442.5 ‰ and -436.7 to -443.2 ‰ (Table 1), as would be expected for MIS 20 based on more recent glacials. In the co-isotopic δD-δ^{18}O diagram of Figure 2a, all samples align well with those from the previous climatic cycles, with a slope of 8.5, close to the value of 8.2 for the samples above 3200m, i.e. in accordance with a meteoric Water Line. This is very different from the refrozen Vostok lake ice, where the samples were shown to be clearly located on a freezing slope of 4.9, only

261 slightly higher than the theoretical slope calculated from the estimated lake water
262 isotopic value (Souchez et al., 2002a). Also, the d_{excess} values shown in Figure 2b are
263 within the range of those observed in the more recent glacials, while refreezing
264 processes are known to lower the deuterium excess values (Souchez et al., 2002a,
265 Souchez and Lorrain, 1991). These are first arguments to preclude large scale
266 refreezing as a plausible process for the bottom ice formation.
267 The gas properties of the bottom ice are probably even more indicative of a true climatic
268 signature (Fig. 3a). The total gas content is very stable with a mean value at 0.088
269 $ml_{air}g^{-1}_{ice}$, which is identical to the one obtained for the whole 0-400 ky interval further up
270 in the core (Raynaud et al., 2007). CH_4, N_2O and CO_2 concentrations are also quite
271 stable and typical of mild to full glacial conditions (mean values of respectively 417
272 ppbv, 247 ppbv and 193 ppmv).$\delta O_2/N_2$ (Table S1) are also typical of meteoric ice with
273 values similar to those described in Landais et al. (2012, their Figure 1, -25°C values).
274 They show no sign of alteration from potential solubility fractionation, as would be
275 expected in the case of significant melting-refreezing processes. Although they show
276 much larger variations, most of insoluble dust concentrations also typically lie within the
277 boundaries of a full glacial state (Fig. 3b).
278 Table 1 gives the mean concentration values of the considered suite of chemical
279 species. A systematic comparison of the mean clean and dispersed ice facies values to
280 those of each of the previous full glacial episodes (with similar δD ranges) shows a very
281 close compatibility, further suggesting that the mean paleoclimatic signal was not
282 modified in the vicinity of the ice-bedrock interface. Indeed, any large-scale regelation
283 process of meteoric ice meltwater would induce significant departure of the chemical

composition (both in terms of total impurity content and of chemical speciation) of the refrozen ice from the initial values present in the meteoric ice. De Angelis et al. (2005, 2004) showed that, in the case of refreezing of the Lake Vostok water, away from any sediment source (their ice type 2), the concentrations were significantly lower than those in meteoric ice, in accordance with the efficient rejection of impurities during freezing at very low rates. Conversely, the upper part of the Vostok lake ice, that is thought to have accreted in a shallow bay upstream of Vostok (ice type 1), shows a total ionic content 5 to 50 times higher than meteoric ice, with a specific signature suggesting contamination from salts originating from deeper sedimentary strata, close to evaporites in composition. Neither of these two signatures are seen in the EDC bottom ice samples.

5.2. Indicators of a “disturbed” paleoclimatic record

There are however some features of the bottom ice that raise questions about its paleoclimatic significance. First of all, as stated above, the presence of visible solid inclusions aggregates in the lower 12 meters could be the result of incorporation processes of sedimentary material at the ice-bedrock interface (Boulton, 1979, , 1996, Cuffey et al., 2000, Gow et al., 1979, Gow and Meese, 1996, Herron and Langway, 1979, Holdsworth, 1974, Iverson, 1993, Iverson and Semmens, 1995, Knight, 1997, Koerner and Fisher, 1979, Souchez et al., 1988, Souchez et al., 2000b, Tison and Lorrain, 1987, Tison et al., 1993, Tison et al., 1989). Then, comparison of Figure 1c and 1e reveals a strong discrepancy between the EDC δD record and the benthic record stack of Lisiecki and Raimo (2005) prior to 800 ky, with the lack of MIS21 in the EDC

306 profile which, instead, displays an unusually long glacial period. Furthermore, the
307 $\delta^{18}O_{atm}$ profile of Figure 1d is also somewhat peculiar, in two ways: first it is extremely
308 stable in the bottom ice despite known large fluctuations in the precession and ice
309 volume at the time, to which the $\delta^{18}O_{atm}$ was shown to be very sensitive (Bender, 2002,
310 Dreyfus et al., 2007, Landais et al., 2010), and, second, it displays values continuously
311 close to 0‰, which is generally (but not strictly) more typical of full interglacial rather
312 than full glacial conditions.
313 Finally, although generally coherent with the previous climatic cycles in terms of mean
314 concentration values, individual chemical species can be considered as two groups with
315 specific and contrasted chemical distribution (Figure 4 and 5, Table 1). MSA, SO_4, Ca
316 and Mg, on the one hand, clearly show increased variability, both in the clean and
317 dispersed ice facies (see left column of Fig. 4 and 1σ values in Table 1), a trend that
318 seems to initiate in MIS18 already. The frequency distributions in Figure 5 confirm this
319 variability as compared to previous glacials, with a tendency of both skewing towards
320 lower values for MSA, SO_4 or Mg and showing outliers at higher concentration,
321 especially in the clean ice facies. On the other hand, Na, K, Cl, and NO_3 behave
322 noticeably differently in the clean ice and in the dispersed ice facies (right column in
323 Figure 4). The clean ice facies (solid line) shows very low variability and narrow
324 frequency peaks in the graphs of Figure 5, while the dispersed ice facies (dotted line)
325 behaves similarly to the previous glacial, but with a tendency of skewing towards the
326 higher range of concentrations.

327 5.3. Distribution and relocation of dissolved and solid impurities within ice cores

Ohno et al. (2005) discussed the location and chemical forms of water-soluble salts in ice cores. Initially entrapped in-between the snow grains that will evolve into firn and then ice under increasing metamorphism, these impurities could therefore be found either within the ice crystals themselves, or within the unfrozen liquid that separates the grain boundaries as a result of "premelting" (Rempel et al., 2001, Rempel et al., 2002, Wettlaufer, 1999), be it veins, nodes or triple junctions. A common view amongst glaciologists is that because those impurities produce strain-energy within ice grains and because trace acids must exist as acid solutions given their very low eutectic point, they will progressively be forced into grain boundaries as grain growth and recrystallization occur (Glen et al., 1977, Rempel, 2003, Rempel et al., 2001, Rempel et al., 2002, Wettlaufer, 1999). Although most of the sulfur atoms present as sulfuric acid in Antarctic ice samples were observed at triple junctions of grain boundaries in the early days of scanning electron measurements in ice (Mulvaney et al., 1988), there has been growing evidence that sulfur compounds also exist as sulfate trapped as inclusions within grains (e.g. Baker and Cullen, 2003). Ohno et al. (2005), using micro-Raman spectroscopy, underline that at shallow depth (185m) in the Dome Fuji ice core, the fraction of SO_4^{2-} existing as salts within the micro-inclusions exceeded 50% of the total SO_4^{2-}. Similar fraction values between 30% and 60% were found for Na^+, Ca^{2+} and Mg^{2+} in discrete samples spanning the 5.6 to 87.8 ky BP interval.

Relocation of impurities under increasing recrystallization, is likely to become important in the deeper part of meteoric ice cores, where the ice temperature gets closer to the pressure melting point (pmp) and the temperature gradient generally increases. One of those relocation processes, that has been intensively discussed in the recent years, is

the mechanism often referred to as “anomalous diffusion” (Rempel, 2003, Rempel et al., 2001, Rempel et al., 2002). In this process, it is surmised that, as grains slowly grow and recrystallize within ice sheets, most of the impurity molecules are preferentially excluded from the solid grains and enriched in the melt. As the polycrystalline mixture of ice and premelt liquid solution flows downwards under gravity at a velocity “v”, it encounters gradual variations in temperature leading to gradients in intergranular concentrations which, in turn, drive molecular diffusion of solutes relative to the porous ice matrix. The net result is that the bulk impurity profile will move downwards at a rate that differs by a finite “anomalous velocity” v_c from the downwards velocity “v” of the ice itself. A typical modeling case study for the conditions at the location of the GRIP ice core predicts separation of the bulk-impurity profile from the contemporaneous ice by a maximum amount of about 90 cm in the bottom layers (3028m). However, Barnes and Wolff (2004) suggested that the anomalous velocity calculated in Rempel’s model is largely overestimated, since the latter mainly surmises that all impurities are located at triple junctions. As underlined by these authors, if impurities transit at two-grain boundaries, then v_c would be much lower. Also, Ohno et al. (2005), as discussed above, demonstrated that much of these impurities are distributed within the crystal itself, further potentially hampering the “anomalous diffusion” process, as recognized by Rempel (2003). Another important feature of this migration process is that the amplitude of the concentration changes should not be altered, even in the case of asynchronous initial deposition of different species with contrasted concentration levels (Rempel, 2003) . It is therefore difficult to invoke anomalous diffusion to explain the contrasts in

species concentration variability observed in our bottom ice at EPICA Dome C (see 4.2.).

Another interesting process discussed by Rempel (2005), is the one in which the density difference between intercrystalline interstitial water (premelt) and ice produces a hydraulic gradient that drives a downwards liquid flow. When the temperature rises towards the glacier bed, the associated permeability increase leads to more rapid fluid transport, internal melting supplying the changing flow. Although the author shows that, in the specific case where the lower region of the glacier floats on a subglacial reservoir, a reduction in the hydraulic gradient results from surface energy effects and causes a decreasing transport rate in the lower few tens of centimeters, the process mentioned above provides a potential mechanism for downwards migration of the chemical compounds accumulated in the premelt layer as recrystallization at high temperature proceeds.

Finally, it is also worth looking at the few detailed studies on impurity distribution within the accreted lake ice of Lake Vostok (de Angelis et al., 2005, de Angelis et al., 2004). Although the form (solid vs. dissolved) and origin of these impurities might differ from those found in meteoric ice above, both ice types (bottom meteoric ice at EDC and accreted ice at Vostok) were submitted to intense recrystallization at high temperatures (>-5°C), potentially involving impurity relocation. Indeed, a strong 10-fold increase of grain size is observed in the EDC bottom ice - Figure 6, and huge - several tens of cm in size- crystals are reported at Vostok (Montagnat et al., 2001). It is interesting to note that the high-resolution spatial distribution of impurities in both EDC (bottom) and Vostok (lake) ice present striking similarities. Indeed, fine-scale (1 cm) analyses of ion

concentration in accreted ice samples at Vostok (e.g. Fig. 5 in de Angelis et al., 2004) show that Cl, Na, F and NO_3 have a uniform distribution throughout the samples, while SO_4, Ca and Mg are much more heterogeneous. This is clearly the behavior we underlined in our EDC bottom ice (Figures 4 and 5): much higher variability in the basal ice than in the meteoric ice above, and much higher variability for SO_4, Ca, Mg and MSA (ion absent in Vostok refrozen ice due to lake water concentration) than for Na, K, Cl and NO_3 in both the clean and dispersed basal ice facies. In the case of the Vostok accreted ice, de Angelis et al. (2005) observed that Cl, Na and K are incorporated within bubble shaped structures, very likely brine micro-pockets refrozen during the core extraction, while SO_4, Ca and Mg are present in aggregates of insoluble material (initially suspended in the lake water),all impurities being originally randomly distributed within the unconsolidated frazil ice lattice. These authors then surmise that, as consolidation, grain growth and recrystallization occur at high temperature (-3°C), brine micro droplets containing soluble salt ionic species like Cl^-, Na^+ or K^+ are not relocated and remain homogeneously distributed throughout the ice lattice, while ions associated to fine solid salt particles, are excluded and gathered with other mineral particles in inclusions of increasing sizes, leading to a greater heterogeneity. Although SO_4 salts and associated species clearly could not initially exist as a suspension in lake water in the EDC case (where refreezing of a water body is inconsistent with the isotopic and gas data sets (see 4.1. above)), they may be formed through in situ chemical reactions and a similar relocation process of atmospheric inputs under recrystallization could have been at work (see 5.4. below).

5.4. Scenarios for the build-up and evolution of the EPICA deep and basal ice

5.4.1. Mixing?

We saw in the previous sections that some of the properties of the EDC bottom ice are consistent with a pristine paleoclimatic record, while others raise some suspicion. We also demonstrated that significant net refreezing of a water body at the bottom of the ice sheet can be discarded. Another set of processes that were shown to alter the basal ice properties is mixing or folding under enhanced deformation close to the ice-bedrock interface (Souchez, 1997, Souchez et al., 1998, Souchez et al., 1995b, Souchez et al., 2003). Among the anomalies in EDC bottom ice properties, the stability of the δD profile for an unusual period of time, if we trust the EDC time scale and compare our data to the Lisiecki and Raymo benthic record (Fig.1c, e), is probably the most prominent. Homogenization through mixing is a process that was invoked by Souchez et al. (2002a, 2002b) to explain the isotopic properties of the 3400-3538m Vostok depth interval, just above the meteoric-lake ice interface. They indeed show that the δD values are there bracketed in a tight range corresponding to mean values between glacial and interglacial, and that the deuterium excess variability is also strongly reduced. This was supported by the ionic signature showing a narrow range of concentrations corresponding to ice formed under mild glacial conditions. If this was the case for the EDC bottom ice, we should expect, from the comparison of Figures 1c and 1e, that the bottom ice shows mean isotopic values between those of MIS20 and MIS21 in Figure 2b. However, the bottom ice is truly of glacial signature. Also, samples from the basal ice span the whole glacial deuterium excess range.

Mixing with a local isotopic end-member inherited from a previous or initial ice sheet configuration is also unlikely. It was only described for basal ice condition largely below the pmp (see section 1) and generally showed contrasting properties between the present-day ice sheet ice and the local end-member, with a whole range of intermediate values in the mixing zone.

5.4.2. Stretching?

If mixing is therefore improbable at EDC, another mechanical way of explaining the abnormal length of MIS20 is relative vertical stretching under changing stress conditions, i.e. alteration of the stratigraphic time scale. Although, given the location chosen for the EPICA Dome C drilling, stress conditions should be (and are) essentially those of vertical uniaxial compression, Durand et al. (2008) indicate that the fabrics in layers of larger mean crystal sizes (about 6 mm) below 2850 meters show signs of dispersion of the strong single maximum (which is the rule below 1500m depth) along a weak vertical girdle. These changes might be the sign of evolving stress conditions near the bottom of the ice sheet, and were recently interpreted so, to explain anomalous flow below 2700m (Dreyfus et al., 2007) and reworking of sulphate spikes below 2800m under increased recrystallization (Traversi et al., 2006; Traversi et al., 2009).
As seen on the large scale map of the bedrock elevation in the vicinity of the EDC drilling site (Remy and Tobacco, 2000, their Figure 4), the ice core bottom location sits at ca. 70 m above sea level, on the eastern flank (200-400 m a.s.l. ridge) of a major S-N trending subglacial valley, with a 400 m a.s.l. ridge 15 km across, on the western flank

of the valley. The bottom of the central part of the valley is at ca. 50 meters below sea level. The next 400 meters deep subglacial valley lies about 20 km further to the East. In Figure 7, we schematically show what might be the impact of a confining bedrock topography consisting of elongated valleys about 20 km wide and 200-400 meters deep (Rémy and Tabacco, 2000) on the stress field and the ice fabric in the bottom ice of EPICA DC. As the ice sinks passed the crests of the subglacial valleys, lateral compression on the sides of the valley will progressively combine with the vertical uniaxial compression. The resulting stress field, will therefore transition from uniaxial vertical compression to longitudinal extension, as illustrated by the 3D-arrows in the central part of the drawing of Figure 7. The associated change in fabrics will be from a vertical single maximum to a vertical girdle fabric, in a plane parallel to the subglacial valley sides. This new pattern might be the one already suggested in the discretely changing fabrics described by Durand et al. (2008) below 2800 meters. Because the principal stress transverse to the subglacial valley slowly shifts from extensional to compressive, the result could be a *relative* vertical stretching of individual accumulation layers, depending on the intensity of the principal extension along the valley axis. It is however not possible, with the data at hand, to demonstrate wether this relative vertical stretching results in an absolute increase of annual layer thickness (as shown in Figure 7) or if it only results in a decrease of the thinning rate. In this configuration, one must of course consider a 3-D geometry, in which the vertically stretched ice can be moved away from the drill location. Part of it can be melted at the ice-bedrock interface where the ice is at the pressure-melting point, and the over-deepening of the longitudinal

valleys seen in Figure 3 of Rémy and Tobacco (2000) could also provide an escape route for the ice.

5.4.3. Enhanced recrystallization and small scale chemical sorting

In the dynamic context described above (5.4.2), and relying on our multiparametric results, we can now propose a plausible scenario for the evolution of the properties of our clean and dispersed basal ice facies at EPICA Dome C, as illustrated in Figure 8. A changing stress field and the high temperatures, close to the pmp, will trigger sustained migration recrystallization within the bottom layers. Mean crystal size values (up to more than 10 cm) plotted in Figure 6 are undisputable proof that recrystallization is indeed very active there. This process will tend to relocate the impurities at grain boundaries and contribute to the build-up of aggregates. Note that Raisbeck et al. (2006) already invoked the formation of aggregates to explain abnormal spikes in ^{10}Be in the basal ice. Increasing water content in the premelt layer might also slowly initiate downwards density-driven migration of the water and of some of the associated impurities. This however, as our data set shows, will only be revealed in a high resolution chemistry approach, since it will not significantly affect the mean concentration values for a given climatic period, but more the frequency distribution within the observed concentration range. It will also behave differently, depending on the species. Detailed SEM and XRF micro-probe elemental analyses of individual aggregates inside the EDC dispersed basal ice facies are described elsewhere and provide further insights in the potential processes at work and environmental implications (de Angelis et al., 2013). They reveal that $CaCO_3$ and $CaSO_4$ are common within these aggregates. These compounds could

509 then be either newly precipitated salts (as observed concentrations are compatible with
510 saturation for e.g. $CaSO_4$ given estimated vein sizes at those ambient temperatures) or
511 pre-existing solid particles, that were initially present inside the crystals (Ohno et al.,
512 2005). SO_4, Ca, Mg and MSA (which can also be associated with salts, Ohno et al.,
513 2005) mean concentrations in the clean and the dispersed basal ice facies will therefore
514 remain within the range of other glacials, but their spatial distribution at the high-
515 resolution scale of sampling, will show much greater variability than in meteoric ice
516 above (Figures 4, 5 and 8-right column).
517 As discussed above, the other group of species (Na, Cl, K, NO_3) shows two important
518 features in the frequency distribution of Figure 5 (right column): a) although the whole
519 data set is spanning the range of the previous glacials, the concentration mode is lower
520 for the clean ice facies and higher for the dispersed ice facies and b) the frequency
521 distribution in the basal ice facies is generally single-modal and narrow, while it is bi-
522 modal in the dispersed ice facies with the first mode in the basal ice facies range and
523 the second mode skewed towards the high side of the range observed in other glacials.
524 The contrast in concentration level between the clean ice facies and the dispersed ice
525 facies could simply reflect the slightly colder conditions (thus higher impurity content) at
526 the time the ice of the dispersed basal facies was formed at the surface of the ice sheet,
527 as suggested by the lower δD values compared to the clean ice facies(Fig. 1b).
528 Although this contrast is less obvious for the first group of chemical compounds, it might
529 have been there over-written by the invoked aggregation and new in-situ precipitation
530 processes. Alternatively, the observed contrast in behavior of Na, Cl, K, NO_3 between
531 the clean and dispersed ice facies might reflect the signature of the premelt migration

process as theoretically put forward by Rempel (2005). These species would indeed remain in the dissolved state within the premelt layer, and eventually partly and more easily migrate downwards, resulting in the left skewing mode in the clean ice facies and the bimodal distribution in the dispersed ice facies (low concentration mode corresponding to the remaining fraction in crystals as salts micro-inclusions and high concentration mode to the fraction that migrated in the premelt). Note that the process of upwards pulling of liquid from the underlying reservoir discussed by Rempel (2005), if it exists, provides a means to prevent expulsion of the premelt from the basal ice, and therefore preservation of this bi-modal frequency distribution. Basal melting would potentially counteract this effect but the two basal ice facies would then migrate upwards into the ice column. Unfortunately, as underlined before, the available data set is missing the lower 6-15 meters of the basal ice section to the ice-bedrock interface, where further arguments might have been found to (in-) validate this premelt migration hypothesis.

The large inclusions visible in the bottom 12 meters of basal ice are principally located at grain boundaries. Theoretical considerations from Alley et al. (1986, eq. 21) suggest a high velocity ice grain boundary migration regime, with decoupling of the grain boundaries from the particle aggregates, because of their relatively large sizes and very low volume fraction. However, as underlined by these authors, this is probably no more valid for the “warm” (EDC bottom) ice, in a full migration recrystallization process, where the increased water content in the vein network will favor Ostwald ripening as the temperature of the ice-impurity system rises above the melting point of the impure grain boundaries. Another feature to consider here is that the particle aggregates might also

555 behave very differently from single particles in terms of drag force on the grain
556 boundaries. Also, as discussed in de Angelis et al. (2013), the significant contribution of
557 organic compounds (such as exopolymeric substances - EPS) to the impurity load might
558 also strongly affect the inclusion/grain boundary geometrical relationships.
559
560 *5.4.4. Water isotopes, gases and dust*
561
562 We focused until now on a plausible explanation for the peculiarities of the chemical
563 signature of our two basal ice facies at EDC. How do the water isotopes signature, gas
564 and dust properties fit into the proposed mechanism? Although the water co-isotopic
565 signature of our basal ice facies does not show large scale signs of modification, the
566 recent work of Pol et al. (2010) suggests that it might not be the case at the crystal size
567 scale, thereby providing some independent support to the interpretation of our chemical
568 data set. These authors indeed used high-resolution (cm scale) δD measurements to
569 depict abnormal isotopic diffusion which they attributed to water circulation at grain
570 boundaries (premelt) for large crystals which spent more than 200.000 years at
571 temperatures >-10°C. The diffusion length diagnosed from the data is about twice larger
572 (40 cm) than expected from solid state diffusion in ice, and it is also suggested that the
573 process might start as early as in MIS 11 (Pol et al., 2011).
574 Why would the relocation process invoked for the chemical impurities not show up in the
575 total air content or the CH_4 and CO_2 concentrations? First of all, it should be noted that
576 the resolution of our gas data sets is much lower than the one we achieved for the
577 chemical species. Also, one should remember that the gas molecules are exclusively

present as clathrates at these depths and little is known on the behavior of those during small-scale phase changes under large overburden pressures. If the glacial MIS20 "stretching" hypothesis is valid, it is not surprising to observe a stable $\delta^{18}O_{atm}$ signal. Landais and Dreyfus (2010) provide an in depth analysis of the potential drivers for the millennial and orbital variations of $\delta^{18}O_{atm}$ and show the strong impact of Northern Hemisphere monsoon activity on the observed values, in response to precessional and millennial shifts of the Intertropical Convergence Zone (ITCZ). Intervals where $\delta^{18}O_{atm}$ is close to 0‰ correspond in that context to episodes where precession favors warm northern hemisphere summers with a strong East-Asian monsoon. In Figure 1f, we plotted the values for the integrated summer insolation at 30°N, for various thresholds τ, as calculated by Huybers (2006). This integrated summer insolation can be defined as the sum of the diurnal average insolation on days exceeding a specified flux threshold (τ). As can be seen from the comparison between Figures 1f and 1d, high values of $\delta^{18}O_{atm}$ concur with high integrated summer insolation associated with very high diurnal average insolation thresholds (e.g. for τ = 450 (green curve) to 500 (red curve) $Wattm^{-2}$ in Figure 1f), which is the case for our basal ice sequence. This relationship in enlarged in Figure 9a, where one can clearly see that maxima in $\delta^{18}O_{atm}$ are well coupled to maxima in integrated summer insolation, to the exception of a missing peak around 750 ky. It can also be suggested that larger $\delta^{18}O$ amplitudes correspond to larger summer insolation values and vice versa, with a threshold around roughly 2 GJ. In Figure 9a we attempted to use the synchronicity of small scale oscillations of the $\delta^{18}O_{atm}$ signal (however well above the precision of measurements - 0.015‰), to the summer

insolation one (tie points 1 and 2 in Fig. 9a) to derive the amount of stretching of the basal ice sequence. This gives a factor of about 2, which allowed us to reconstruct a new time scale for the basal ice, assuming linear stretching also applying to the bottom ice, for which $\delta^{18}O_{atm}$ are not available. Unfortunately, this does not resolve the discrepancy with the Lisiecki and Raymo curve (Figure 9b), and suggests that the amount of stretching is probably much larger, with an initial time frame for the basal ice of only about 10.000 years. To build our 60 meters of basal ice sequence in ca. 10000 years would require an "in situ" annual layer thickness of 6 mm, which is 10 times the value observed during the previous glacial, following the recently published AICC2012 climate record (Bazin et al., 2012, supplementary material). This seems too extreme, and suggests stretching might have been supplemented by other processes such as dynamical thickening in the lee of bedrock obstacles or stacking up of several glacials, with missing interglacials. The latter is however unlikely, since interglacial ice is usually harder to deform due to lower impurity content and larger crystal size (Dahl-Jensen et al., 2013). Finally, as demonstrated in de Angelis et al. (2013), the detailed analysis of individual inclusions supports the occurrence of in-situ bacterial activity. To our knowledge, it is not known so far if these might have potential impact on the $\delta^{18}O_{atm}$ of the neighbouring gas phase. It is however unlikely that it might be significant given the observed low CO_2 mixing ratio (Fig. 3a), in line with atmospheric values at glacial times. Despite the very poor resolution of the dust record in our bottom ice the large variability of the data within the glacial range could also result from our increased relocation scheme. Moreover, below 2900m, a significant shift of particle size towards large diameters is in agreement with the formation of aggregates.

6. Conclusions

We used a multiparametric approach to discuss the plausibility of recovering an unaltered paleoclimatic signature from the basal ice of the EDC ice core. We showed that some of the data (δD values, total air content, gas composition, dust content, mean chemical species concentrations) suggest a pristine meteoric glacial signature while others (length of the glacial, $\delta^{18}0_{atm}$, visible inclusions, variability of the chemical species distribution) suggest mechanical and compositional alteration of the bottom ice. Ice stable isotopes and total air content rule out large scale refreezing processes of a water reservoir as the origin for the bottom ice. Mixing, be it internally (as in Vostok MIS11) or with a local ice remnant of previous or initial ice sheet configuration (as in GRIP and Dye-3) can be equally discarded.

Using a new high resolution data set for selected chemical species in the basal EDC ice and remote sensing information on the general setting of the Dome C area, we propose a mechanism in which the confining bedrock topography contributes to a downwards change in the stress field from uniaxial vertical compression to longitudinal extension along the valley axis. This stress configuration change results in a potential relative vertical stretching of the ice layers, which explains the abnormal length of MIS20. Combined with an ice temperature close to the pmp it also favors rapid migration recrystallization, as witnessed by the large increase in grain size. This, in turn, induces relocation of impurities, with accumulation of newly formed salts and already existing solid particles in the premelt layer, forming aggregates. Those become visible about 12 meters above the bottom of the core and increase in size and number downwards. The basal inclusions thus mainly consist of reworked existing material, rather than

representing incorporation of allocthonous material from the ice-bedrock interface. However some potential candidates for the latter (large, single, mineral inclusions) were detected in the last meter layer (de Angelis et al., 2013). Although the mean concentration values were not significantly different from those observed in the previous full glacial periods, some chemical sorting is apparent, especially for those species that are not involved in salt formation. We suggest this might result from a slow process of downwards migration of the premelt layer under the hydraulic gradient resulting from the density difference between ice and interstitial water, although the lack of data from the last 6-15 meters to the ice-bedrock interface prevents us from further validating this hypothesis. The ice isotopic and gas properties are apparently not affected by these small scale processes that however only become detectable at high-resolution sampling (sub-crystal size), where they are involved in smoothing processes. The apparent discrepancy in the $\delta^{18}O_{atm}$ signal is resolved if one considers potential stretching of a glacial time span during which precession favors warm northern hemisphere summers, as happened temporarily in each of the previous glacial isotopic stages.

We conclude that the paleoclimatic signal is only marginally affected in terms of global ice properties at the bottom of EPICA Dome C, but that the time scale was considerably distorted by mechanical stretching due to the increasing influence of the subglacial topography. It is interesting to note that MIS18 already shows signs of isotopic smoothing, chemical relocation and increased variability for the species involved in salt formation (MSA, SO_4, Mg and, in a lesser extent Ca), before the timescale (EDC3) got significantly distorted. Along the same line the anomalous flow detected below 2700m, that led to the change from the EDC2 to the EDC3 time scale, might already find its

roots in this subglacial topography distortion, although possible changes in the Dome position with time need also to be considered (e.g. Urbini et al., 2008).Many interior ice divides are indeed migrating today and this could also be the case for the EDC location. Given the rough bed topography, it takes a migration of only a few ice thicknesses to change the bedrock elevation by ca. 200 meters. The basal ice may therefore have experienced vertical stretching due to flow from the bedrock ridge to the current valley position, with recent migration of the divide at the top. Today, lively discussions exist and preliminary actions are undertaken within the ice core community to select a suitable location for a new deep drilling targeting the “oldest ice” (above 1 million years old, IPICS, 2009). Our work shows that the location of the EDC ice core on the flank of a valley-type subglacial topography has considerably affected the inference of deep timescales. We conclude that the retrieving of reliable paleoclimatic signals down to a few meters from the ice-bedrock interface would probably be thinkable on a flat monotonic bedrock, for distances several times the local ice thickness, although small scale reworking of some of the proxies should be expected. It is however not clear yet why the gas content and composition is so well preserved at EDC, and not at other deep basal ice location. The presence of a liquid water layer at the interface might partly explain that discrepancy, although this could not be verified here.

Future work on the EPICA DC bottom ice will involve high resolution gas measurements in selected areas and an in-depth analysis of the crystallographic properties below 3200 meters. Hopefully, these will allow us to validate and refine the general mechanism discussed here.

Acknowledgments

This work is a contribution to the European Project for Ice Coring in Antarctica (EPICA), a joint European Science Foundation/European Commission (EC) scientific programme, funded by the EU (EPICA-MIS) and by national contributions from Belgium, Denmark, France, Germany, Italy, The Netherlands, Norway, Sweden, Switzerland and the UK. The main logistic support at Dome C was provided by IPEV and PNRA. The authors wish to warmly thank B. Hubbard and two anonymous referees for their constructive comments on the “Discussion” version of this manuscript, and D. Raynaud and F. Parrenin for valuable discussions.

References

Alley, R.B., Perepezko, J.H.Bentley, C.R., 1986. Grain growth in polar ice : I. Theory,. J. Glaciol. 32, 415-424.

Baker, I., Cullen, D., 2003. SEM/EDS observations of impurities in polar ice: artefacts or not? J. Glaciol. 49, 184-190.

Bazin, L., Landais, A., Lemieux-Dudon, B. , Toyé Mahamadou Kele, H., Veres, D., Parrenin, F. , Martinerie, P., Ritz, C. , Capron, E. , Lipenkov, V., Loutre, M.-F., Raynaud, D., Vinther, B. , Svensson, A. , Rasmussen, S. O. , Severi, M. , Blunier, T. , Leuenberger, M. , Fischer, H. , Masson-Delmotte, V. , Chappellaz, J. , Wolff, E. 2012. An optimized multi-proxy, multi-site Antarctic ice and gas orbital chronology (AICC2012): 120–800 ka, Clim. of the Past., 9, 1715-1731, 2013

Bender, M.L., 2002. Orbital tuning chronology for the Vostok climate record supported by trapped gas composition. Earth Planet. Sci. Lett. 204, 275-289.

Boulton, G.S., 1979. Processes of erosion on different substrata. J. Glaciol. 23, 15-38.

Boulton, G.S., 1996. Theory of glacial erosion, transport and deposition as consequence of subglacial sediment deformation. J. Glaciol. 42, 43-62.

Chappellaz, J., Blunier, T., Kints, S., Dällenbach, A., Barnola, J.M., Schwander, J., Raynaud, D., Stauffer, B., 1997. Changes in the atmospheric CH4 gradient between Greenland and Antarctica during the Holocene. J. of Geophys. Res.-Atm. 102, 15987-15997.

721 Cuffey, K., Conway, H., Gades, A., Hallet, B., Lorrain, R., Severinghaus, J.P., Steig, E.,
722 Vaughn, B.White, J., 2000. Entrainment at cold glacier beds. Geology 28, 351-
723 354.

724 Dahl-Jensen, D., Albert, M. R., Aldahan, A., Azuma, N., Balslev-Clausen, D., Baumgartner, M.,
725 Berggren, A.-M., Bigler, M., Binder, T., Blunier, T., Bourgeois, J. C., Brook, E. J., Buchardt, S.
726 L., Buizert, C., Capron, E., Chappellaz, J., Chung, J., Clausen, H. B., Cvijanovic, I., Davies, S.
727 M., Ditlevsen, P., Eicher, O., Fischer, H., Fisher, D. a., Fleet, L. G., Gfeller, G., Gkinis, V.,
728 Gogineni, S., Goto-Azuma, K., Grinsted, A., Gudlaugsdottir, H., Guillevic, M., Hansen, S. B.,
729 Hansson, M., Hirabayashi, M., Hong, S., Hur, S. D., Huybrechts, P., Hvidberg, C. S., Iizuka, Y.,
730 Jenk, T., Johnsen, S. J., Jones, T. R., Jouzel, J., Karlsson, N. B., Kawamura, K., Keegan, K.,
731 Kettner, E., Kipfstuhl, S., Kjær, H. a., Koutnik, M., Kuramoto, T., Köhler, P., Laepple, T.,
732 Landais, A., Langen, P. L., Larsen, L. B., Leuenberger, D., Leuenberger, M., Leuschen, C., Li,
733 J., Lipenkov, V., Martinerie, P., Maselli, O. J., Masson-Delmotte, V., McConnell, J. R., Miller, H.,
734 Mini, O., Miyamoto, A., Montagnat-Rentier, M., Mulvaney, R., Muscheler, R., Orsi, a. J., Paden,
735 J., Panton, C., Pattyn, F., Petit, J.-R., Pol, K., Popp, T., Possnert, G., Prié, F., Prokopiou, M.,
736 Quiquet, A., Rasmussen, S. O., Raynaud, D., Ren, J., Reutenauer, C., Ritz, C., Röckmann, T.,
737 Rosen, J. L., Rubino, M., Rybak, O., Samyn, D., Sapart, C. J., Schilt, A., Schmidt, a. M. Z.,
738 Schwander, J., Schüpbach, S., Seierstad, I., et al.: Eemian interglacial reconstructed from a
739 Greenland folded ice core, Nature, 493(7433), 489–494, doi:10.1038/nature11789, 2013.

740 de Angelis, M., Morel-Fourcade, M.-C.B., J.-M., Susini, J.Duval, P., 2005. Brine micro-
741 droplets and solid inclusions in accreted ice from Lake Vostok (East Antarctica).
742 Geophys. Res. Lett. 32, doi: 10.1029/2005GL022460.

743 de Angelis, M., Petit, J.-R., Savarino, J., Souchez, R.Thiemens, M.H., 2004.
744 Contributions of an ancient evaporitic-type reservoir to subglacial Lake Vostok
745 chemistry. Earth Planet. Sci. Lett. 222, 751-765.

746 de Angelis, M., Tison, J.-L. , Morel-Fourcade, M.-C., Susini, J., 2013. Micro-investigation
747 of EPICA Dome C bottom ice : Evidence of long term *in situ* processes involving
748 acid-salt interactions, mineral dust and organic matter, Quat. Sci. Rev., 78, 248-
749 265

750 Delmonte, B., Andersson, P.S., Haqnsson, M., Schöberg, H., Petit, J.-R., Basile-
751 Doelsch, I.Maggi, V., 2008. Aeolian dust in East Antarctica (EPICA-Dome C and

752 Vostok): Provenance during glacial ages over the last 800 kyr. Geophys. Res.
753 Lett. 35, doi:10.1029/2008GRL033382.
754 Dreyfus, G. 2008. Dating an 800,000 Year Antarctic Ice Core Record Using the Isotopic
755 Composition of Trapped Air. (Doctoral dissertation)
756 Dreyfus, G.G., Parrenin, F., Lemieux-Dudon, B., Durand, G., Masson-Delmotte, V.,
757 Jouzel, J., Barnola, J.-M., Panno, L., Spahni, R., Tisserand, A., Siegenthaler,
758 U.Leuenberger, M., 2007. Anomalous flow below 2700m in the EPICA Dome C
759 ice core detected using $\delta^{18}O$ of atmospheric oxygen measurements. Clim. Past
760 3, 341-353.
761 Durand, G., Svensson, A., Persson, A., Gagliardini, O., Gillet-Chaulet, F., Sjolte, J.,
762 Montagnat, M.Dahl-Jensen, D., 2009. Evolution of the texture along the EPICA
763 Dome C ice core. Proceedings of the 2nd International Workshop on Physics of
764 Ice Core records (PICR-2), Hokkaido University, Sapporo, Japan, Institute of Low
765 Temperature Science,
766 EPICA_Community_members, 2004. Eight glacial cycles from an Antarctic ice core.
767 Nature 429, 623-628.
768 Flückiger, J., Blunier, T., Stauffer, B., Chappellaz, J., Spahni, R., Kawamura, K.,
769 Schwander, J., Stocker, T.F., Dahl-Jensen, D., 2004. N_2O and CH_4 variations
770 during the last glacial epoch: Insight into global processes. Glob. Biogeochem.
771 Cycles 18, GB1020, doi:10.1029/2003GB002122.
772 Glen, J.W., Homer, D.R.Paren, J.G., 1977. Water at grain boundaries: its role in the
773 purification of temperate glacier ice. International Association of Hydrological
774 Sciences Publications 118, 263-271.

775 Goodwin, I.D., 1993. Basal ice accretion and debris entrainment within the coastal ice
776 margin, Law Dome, Antarctica. J. Glaciol. 39, 157-166.
777 Gow, A.J., Epstein, S.Sheehy, W., 1979. On the origin of stratified debris in ice cores
778 from the bottom of the Antarctic Ice Sheet. J. Glaciol. 23, 185-192.
779 Gow, A.J.Meese, D.A., 1996. Nature of basal debris in the GISP2 and Byrd ice cores
780 and its relevance to bed processes. Ann. Glaciol. 22, 134-140.
781 Herron, S., Langway, C., 1979. The debris-laden ice at the bottom of the Greenland ice-
782 sheet. J. Glaciol. 23, 193-207.
783 Holdsworth, G., 1974. Meserve Glacier, Wright Valley, Antarctica, part I. Basal
784 processes. n° 37, Institute of Polar Studies, The Ohio State University Research
785 Foundation, Columbus
786 Huybers, P., 2006. Early Pleistocene glacial cycles and the integrated summer
787 insolation forcing, Science 313, 5786, 508-511, 10.1126/science.1125249, 28
788 July 2006
789 International Partnerships in Ice Core Sciences, 2009. IPICS White papers.
790 www.pages-igbp.org/ipics/whitepapers.html
791 Iverson, N.R., 1993. Regelation of ice through debris at glacier beds: Implications for
792 sediment transport. Geology 21, 559-562.
793 Iverson, N.R.Semmens, D., 1995. Intrusion of ice into porous media by regelation: A
794 mechanism of sediment entrainment by glaciers. J. Geophys. Res. 100, 10219-
795 10230.
796 Jouzel, J., Masson-Delmotte, V., Cattani, O., Dreyfus, G., Falourd, S., Hoffmann, G.,
797 Minster, B., Nouet, J., Barnola, J.M., Chappelaz, J., Fischer, H., Gallet, J.C.,

Johnsen, S., Leuenberger, M., Loulergue, L., Luethi, D., Oerter, H., Parrenin, F., Raisbeck, G., Raynaud, D., Schilt, A., Schwander, J., Selmo, E., Souchez, R., Spahni, R., Stauffer, B., Steffensen, J.-P., Stenni, B., Stocker, T.F., Tison, J.-L., Werner, M.Wolff, E.W., 2007. Orbital and Millennial Antarctic Climate Variability over the Past 800,000 Years. Science 317, DOI: 10.1126/science.1141038.

Jouzel, J., Petit, J.R., Souchez, R., Barkov, N., Lipenkov, V., Raynaud, D., Stievenard, M., Vassiliev, N., Verbeke, V.Vimeux, F., 1999. More than 200 meters of lake ice above subglacial lake Vostok, Antarctica. Science 286, 2138-2141.

Knight, P.G., 1997. The basal ice layer of glaciers and ice sheets. Quat. Sci. Rev. 16, 975-993.

Koerner, R.M.Fisher, D.A., 1979. Discontinuous flow, ice texture, and dirt content in the basal layers of the Devon Island Ice Cap. J. Glaciol. 23, 209-221.

Lambert, F., Delmonte, B., Petit, J.-R., Bigler, M., Kaufmann, P.R., Hutterli, M.A., Stocker, T.F., Ruth, U., Steffensen, J.P.Maggi, V., 2008. Dust-Climate couplings over the past 800,000years from the EPICA Dome C ice core. Nature 452, doi:10.1038/nature06763.

Landais, A., Dreyfus, G., Capron, E., Masson-Delmotte, V., Sanchez-Goni, M.F., Desprat, S., Hoffmann, G., Jouzel J., Leuenberger,M., Johnsen, S., 2010. What drives the millennial and orbital variations of $\delta^{18}O_{atm}$?. Quat. Sci. Rev. 29: 235-246

Landais, A., Dreyfus, G., Capron, A., Pol, K., Loutre, M.F., Raynaud, D., Lipenkov, Y., Arnaud, L., Masson-Delmotte, V., Paillard, D., Jouzel, J. , Leuenberger, M., 2012. Clim. Past, 8, 191-203

821 Landais, A., Caillon, N., Severinghaus, J., Jouzel, J., Masson-Delmotte, V., 2003.
822 Analyses isotopiques à haute précision de l'air piégé dans les glaces polaires
823 pour la quantification des variations rapides de température: méthode et limites.
824 Notes des Activités Instrumentales de l'IPSL 39.
825 Lefebvre, E., Ritz, C., Legrésy, B., Possenti, P., 2008. New temperature profile
826 measurement in the EPICA Dome C borehole. Geophysical Research Abstracts,
827 EGU General Assembly 2008, 13-18 April 2008, European Geophysical Union.
828 Lipenkov, V., Candaudap, F., Ravoire, J., Dulac, E., Raynaud, D., 1995. A new device
829 for air content measurements in polar ice. J. Glaciol. 41, 423-429
830 Lisiecki, L.E.Raymo, M.E., 2005. A Pliocene-Pleistocene stack of 57 globally distributed
831 benthic $\delta^{18}O$ records. Paleoceanography 20, doi:10.1029/2004PA001071.
832 Littot, G. C., Mulvaney, R., Röthlisberger, R., Udisiti, R., Wolff, E., Castellano, E., De
833 Angelis, M., Hansson, M., Sommer, S., Steffensen, J.P., 2002.. Comparison of
834 analytical methods used for measuring major ions in the EPICA Dome C
835 (Antarctica) ice core. Ann. Glaciol. 35, 299–-305.
836 Loulergue, L., Schilt, A., Spahni, R., Masson-Delmonte, V., Blunier, T., Lemieux, B.,
837 Barnola, J.-M., Raynaud, D., Stocker, T.F.Chappelaz, J., 2008. Orbital and
838 millennial-scale features of atmospheric CH_4 over the past 800,000 years. Nature
839 453, doi:10.1038/nature06950.
840 Lüthi, D., Le Floch, M., Bereiter, B., Blunier, T., Barnola, J.-M., Siegenthaler, U.,
841 Raynaud, D., Jouzel, J., Fischer, H., Kawamura, K.Stocker, T.F., 2008. High-
842 resolution carbon dioxide concentration record 650,000-800,000 years before
843 present. Nature 453, doi:10.1038/nature06949.

844 Martinerie, P., Lipenkov, V.Y., Raynaud, D., 1990. Correction of air content
845 measurements in polar ice for the effect of cut bubbles at the surface of the
846 sample. J. Glaciol. 36, 299-303
847 Montagnat, M., Duval, P., Bastie, P., Hamelin, B., de Angelis, M., Petit, J.R.Lipenkov,
848 V.Y., 2001. High crystalline quality of large single crystals of subglacial ice above
849 Lake Vostok (Antarctica) revealed by hard X-ray diffraction. C.R. Acad. Sc. Paris,
850 Série IIa Sciences de la Terre et des Planètes 333, 419-425.
851 Mulvaney, R., Wolff, E.W.Oates, K., 1988. Sulphuric acid at grain boundaries in
852 Antarctic ice. Nature 331, 247-249.
853 Ohno, H., Igarashi, M.Hondoh, T., 2005. Salt inclusions in polar ice cores: Location and
854 chemical form of water-soluble impurities. Earth Planet. Sci. Lett. 232, 171-178.
855 Parrenin, F.; Loulergue, L. and Wolff, E. W., 2007 EPICA Dome C Ice Core Timescales
856 EDC3. doi:10.1594/PANGAEA.671367
857 Pickering, F. B.: The basis of Quantificative Metallography., Metals and Metallurgy
858 Trust, 1976.
859 Petit, J., Jouzel, J., Raynaud, D., Barkov, N., Barnola, J.M., Basile, I., Bender, M.,
860 Chappellaz, J., Davis, M., Delaygue, G., Delmotte, M., Kotlyakov, V., Legrand,
861 M., Lipenkov, V., Lorius, C., Pépin, L., Ritz, C., Saltzman, E.Stievenard, M.,
862 1999. Climate and atmospheric history of the past 420,000 years from the Vostok
863 ice core, Antarctica. Nature 399, 429-436.
864 Pol, K., Debret, M., Masson-Delmotte, V., Capron, E., Cattani, O., Dreyfus, G., Falourd,
865 S., Johnsen, S., Jouzel, J., Landais, A., Minster, B, Stenni, B., 2011. Links
866 between MIS 11 millennial to sub-millennial climate variability and long term

trends as revealed by new high resolution EPICA Dome C deuterium data - A comparison with the Holocene. Clim. Past, 7, 437-450

Pol, K., Masson-Delmotte, V., Johnsen, S., Bigler, M., Cattani, O., Durand, G., Falourd, S., Jouzel, J., Minster, B., Parrenin, F., Ritz, C., Steen-Larsen, H.C., Stenni, B., 2010. New MIS 19 EPICA Dome C high resolution deuterium data: Hints for a problematic preservation of climate variability at sub-millennial scale in the "oldest ice", Earth Planet. Sci. Lett., 298, 1-2, 95-103

Raisbeck, G.M., Yiou, F., Cattani, O.Jouzel, J., 2006. ^{10}Be evidence for the Matuyama-Brunhes geomagnetic reversal in the EPICA Dome C ice core. Nature 444, doi:10.1038/nature05266.

Raynaud, D., Lipenkov, V., Lemieux-Dudon, B., Duval, P., Loutre, M.-F.Lhomme, N., 2007. The local insulation signature of air content in Antarctic ice. A new step toward an absolute dating of ice records. Earth Planet. Sci. Lett. 261, 337-349.

Raynaud D., B.J.M., R. Souchez, R. Lorrain, Petit J.-R., Duval P., Lipenkov V., 2005. The record for marine isotopic stage 11. Nature 436, 30-40.

Rempel, A., 2005. Englacial phase changes and intergranular flow above subglacial lakes. Ann. Glaciol. 40, 191-194.

Rempel, A.W., 2003. Segregation, transport and interaction of climate proxies in polycrystalline ice. Can. J. Phys. 81, 89-97.

Rempel, A.W., Waddington, E.D., Wettlaufer, J.S.Worster, M.G., 2001. Possible displacement of the climate signal in ancient ice by premelting and anomalous diffusion. Nature 411, 568-571.

889 Rempel, A.W., Wettlaufer, J.S.Waddington, E.D., 2002. Anomalous diffusion of multiple
890 impurity species: predicted implications for the ice core climate record. J.
891 Geophys. Res. ,107, B12, DOI: 10.1029/2002JB001857
892 Rémy, F.Tabacco, I.E., 2000. Bedrock features and ice flow near the EPICA ice core
893 site (Dome C, Antarctica). Geophys. Res. Lett. 27, 405-408.
894 Schilt, A., Baumgartner M., Blunier T., Schwander J., Spahni R., Fischer H., and
895 Stocker, T.F., 2010., Glacial-interglacial and millennial-scale variations in the
896 atmospheric nitrous oxide concentration during the last 800000 years, Quat. Sci.
897 Rev. (2010), doi:10.1016/j.quascirev.2009.03.011
898 Souchez, R., 1997. The build up of the ice sheet in Central Greenland, Journal of
899 Geophysical Research. J. Geophys. Res. 102, 26317-26323.
900 Souchez, R., Bouzette, A., Clausen, H., Johnsen, S.Jouzel, J., 1998. A stacked mixing
901 sequence at the base of the Dye 3 core, Greenland. Geophys. Res. Lett. 25,
902 1943-1946.
903 Souchez, R., Janssens, L., Lemmens, M.Stauffer, B., 1995a. Very low oxygen
904 concentration in basal ice from Summit, Central Greenland. Geophys. Res. Lett.
905 22, 2001-2004.
906 Souchez, R., Jean-Baptiste, R., Petit, J.R., Lipenkov, V.Jouzel, J., 2002a. What is the
907 deepest part of the Vostok ice core telling us ? Earth Sci. Rev. 60, 131-146.
908 Souchez, R., Jouzel, J., Landais, A., Chapellaz, J., Lorrain, R.Tison, J.-L., 2006. Gas
909 isotopes in ice reveal a vegetated central Greenland during ice sheet invasion.
910 Geophys. Res. Lett. 33 L24503.

911 Souchez, R., Lemmens, M.Chappellaz, J., 1995b. Flow-induced mixing in the GRIP
912 basal ice deduced from the CO_2 and CH_4 records. Geophys. Res. Lett. 22 41-44
913 Souchez, R., Lemmens, M., Tison, J.-L., Lorrain, R.Janssens, L., 1993b. Reconstruction
914 of basal boundary conditions at the Greenland Ice Sheet margin from gas
915 composition in the ice. Earth Planet. Sci. Lett. 118, 327-333.
916 Souchez, R.Lorrain, R., 1991. Ice composition and glacier dynamics, 207 pp.
917 Heidelberg, Springer-Verlag, 0 387 52521 1
918 Souchez, R., Lorrain, R., Tison, J.-L., Jouzel, J., 1988. Co-isotopic signature of two
919 mechanisms of basal-ice formation in Arctic outlet glaciers. Ann. Glaciol. 10, 163-
920 166.
921 Souchez, R., Petit, J.-R., Jouzel, J., de Angelis, M., Tison, J.L., 2003. Reassessing
922 Lake Vostok's behaviour from existing and new ice core data. Earth Planet. Sci.
923 Lett. 217, 163-170.
924 Souchez, R., Petit, J.R., Jouzel, J., Simões, J., de Angelis, M., Barkov, N., Stievenard,
925 M., Vimeux, F., Sleewaegen, S., Lorrain, R., 2002b. Highly deformed basal ice in
926 the Vostok core, Antarctica. Geophys. Res. Lett. 29, 40.41-40.44.
927 Souchez, R., Petit, J.R., Tison, J.L., Jouzel, J.Verbeke, V., 2000a. Ice formation in
928 subglacial Lake Vostok, Central Antarctica. Earth Planet. Sci. Lett. 181, 529-538.
929 Souchez, R., Tison, J.L., Lorrain, R., Janssens, L., Stievenard, M., Jouzel, J.,
930 Sveinbjörnsdottir, A.Johnsen, S.J., 1994. Stable isotopes in the basal silty ice
931 preserved in the Greenland Ice Sheet at Summit; Environmental implications.
932 Geophys. Res. Lett. 21, 693-696.

933 Souchez, R., Vandenschrick, G., Lorrain, R.Tison, J.-L., 2000b. Basal ice formation and
934 deformation in Central Greenland : a review of existing and new ice core data. In:
935 A. J. Maltman, Hubbard, B., Hambrey, M. (Eds.), Deformation of Glacial
936 Materials, Special Publication n°176, 13-22.
937 Stenni, B., Masson-Delmotte, V., Selmo, E., Oerter, H., Meyer, H., Rothilsberger, R.,
938 Jouzel, J., Cattani, O., Falourd, S., Fisher, H., Hoffmann, G., Iacumin, P.,
939 Johnsen, S., Minster, B., Udisti, R., 2010. The deuterium excess records of
940 EPICA Dome C and Dronning Maud Land ice cores (East Antarctica), Quat. Sci.
941 Rev. 29 (2010) 146–159
942 Tabacco, I.E., Passerini A., Corbelli, F., Gorman, M., 1998. Determination of the surface
943 and bed topography at Dome C, East Antarctica, J. Glaciol. 44, 185-191.
944 Tison, J.-L., Lorrain, R., 1987. A mechanism of basal ice layer formation involving major
945 ice-fabrics changes. J. Glaciol. 33, 47-50.
946 Tison, J.-L., Petit, J.R., Barnola, J.M.Mahaney, W.C., 1993. Debris entrainment at the
947 ice-bedrock interface in sub-freezing temperature conditions (Adélie Land,
948 Antarctica). J. Glaciol. 39, 303-315.
949 Tison, J.-L., Souchez, R.Lorrain, R., 1989. On the incorporation of unconsolidated
950 sediments in basal ice : present-day examples. Zeit. Geomorph. 72, 173-183.
951 Tison, J.-L., Souchez, R., Wolff, E.W., Moore, J.C., Legrand, M.R.de Angelis, M., 1998.
952 Is a periglacial biota responsible for enhanced dielectric response in basal ice
953 from the Greenland Ice Core Project ice core ? J. Geophys. Res., 1998 103,
954 18885-18894.

955 Tison, J.-L., Thorsteinsson, T., Lorrain, R.Kipfstuhl, J., 1994. Origin and development of
956 textures and fabrics in basal ice at Summit, Central Greenland. Earth Planet. Sci.
957 Lett. 125, 421-437.
958 Traversi, R., Becagli, S., Castellano, E., Marino, F., Severi, M., Udisti, R., Kaufmann, P.,
959 Lambert, F., Stauffer, B., Hansson, M., Petit, J.R., Ruth, U., Raisbeck, G.Wolff,
960 E.W., 2006. Chemical characterization of peculiar ice layers at the bottom of the
961 EPICA-DC ice core. Geophysical Research Abstracts, 8, 07199. European
962 Geosciences Union General Assembly 2006, 02-07 April 2006, EGU.
963 Traversi, R., Becagli, S., Castellano, E., Marino, F., Rugi, F., Severi, M., de Angelis, M.,
964 Fisher, H., Hansson, M., Steffensen, J.P., Wolff, E.W., Udisti, R., 2009. Sulfate
965 spikes at the bottom of the EDC core: evidence of glaciological artefacts, Env.
966 Sc. tech., 43, 23, 8737-8743.
967 Urbini, S., Frezzotti, M., Gandolfi, S., Vincent, C., Scarchilli, C., Vittuari, L. Fily, M.,
968 2008. Historical behaviour of Dome C and Talos Dome (East Antarctica) as
969 investigated by snow accumulation and ice velocity measurements. Glob. Planet.
970 Change 60 (2008) 576–588
971 Verbeke, V., R. Lorrain, Johnsen S.J., J.-L. Tison, 2002. A multiple-step deformation
972 history of basal ice from the Dye3 (Greenland) core : new insights from the CO_2
973 and CH_4 content. Ann. of Glaciol. 35, 231-236.
974 Weis, D., Demaiffe, D., Souchez, R., Gow, A.J.Meese, D.A., 1997. Nd, Sr and Pb
975 isotopic compositions of basal material in Central Greenland : inferences for ice
976 sheet development. Earth Planet. Sci. Lett. 150, 161-169.

977 Wettlaufer, J.S., 1999. Impurity effects in the Premelting of ice. Phys. Rev. Lett. 82,
978 2516-2519.
979 Wolff, E.W., Fisher, H., Fundel, F., Ruth, U., Twarloh, B., Littot, G.C., Mulvaney, R.,
980 Röthlisberger, R., de Angelis, M., Boutron, C.F., Hansson, M., Jonsell, U.,
981 Hutterli, M.A., Lambert, F., Kaufmann, P., Stauffer, B., Stocker, T.F., Steffensen,
982 J.P., Bigler, M., Siggaard-Andersen, M.L., Udisti, R., Becagli, S., Castellano, E.,
983 Severi, M., Wagenbach, D., Barbante, C., Gabrielli, P.Gaspari, V., 2006.
984 Southern Ocean sea-ice extent, productivity and iron flux over the past eight
985 glacial cycles. Nature 440, doi:10.1038/nature04614.
986

Tables

Glacial	Depth range (m)		Isotopic range (δD ‰)		MSA (ngg^{-1})		SO_4 (ngg^{-1})		Ca (ngg^{-1})		Mg (ngg^{-1})	
			min	max	mean	*s*	mean	*s*	mean	*s*	mean	*s*
MIS 2	507.7	583.5	-449.3	-432.8	**18.24**	*7.00*	**213.78**	*85.15*	**43.27**	*14.89*	**19.31**	*4.08*
MIS 4	1007.6	1042.2	-446.4	-430.5	**20.94**	*4.00*	**194.80**	*52.52*	**30.85**	*10.96*	**14.28**	*3.84*
MIS 6	1801.8	1997.0	-447.1	-419.8	**18.60**	*5.00*	**170.01**	*51.73*	**23.60**	*12.25*	**13.54**	*4.04*
MIS 8	2320.0	2398.6	-444.5	-421.5	**27.90**	*6.13*	**192.05**	*50.92*	**23.37**	*12.98*	**14.92**	*4.28*
MIS 10	2599.9	2650.0	-445.0	-425.1	**26.77**	*7.88*	**183.55**	*43.56*	**22.92**	*9.84*	**14.92**	*3.86*
MIS 12	2783.2	2794.9	-440.9	-422.5	**23.44**	*5.04*	**187.36**	*45.54*	**43.47**	*19.09*	**19.82**	*5.50*
MIS 14.2	2915.7	2919.9	-436.4	-429.3	**23.75**	*6.37*	**162.06**	*21.72*	**20.46**	*6.19*	**15.80**	*2.75*
MIS 16	3037.6	3039.8	-441.0	-412.3	**32.61**	*6.95*	**167.86**	*39.55*	**36.09**	*17.21*	**16.37**	*5.84*
MIS 18	3137.8	3153.1	-441.4	-423.7	**36.40**	*23.47*	**195.35**	*139.18*	**31.26**	*19.76*	**20.03**	*25.47*
Clean Facies	3201.0	3248.0	-442.5	-427.7	**21.50**	*20.32*	**150.39**	*107.98*	**29.53**	*16.87*	**11.49**	*12.48*
Dispersed Facies	3248.0	3259.3	-443.2	-436.7	**25.27**	*18.43*	**139.58**	*91.46*	**42.10**	*29.44*	**16.25**	*11.23*

Glacial	Depth range (m)		Isotopic range (δD ‰)		Na (ngg^{-1})		Cl (ngg^{-1})		NO_3 (ngg^{-1})		K (ngg^{-1})	
			min	max	mean	*s*	mean	*s*	mean	*s*	mean	*s*
MIS 2	507.7	583.5	-449.3	-432.8	**97.37**	*17.54*	**160.68**	*48.64*	**40.93**	*16.01*	**7.45**	*1.89*
MIS 4	1007.6	1042.2	-446.4	-430.5	**79.81**	*17.75*	**129.89**	*25.25*	**29.38**	*12.41*	**4.91**	*2.34*
MIS 6	1801.8	1997.0	-447.1	-419.8	**71.57**	*16.65*	**107.56**	*40.45*	**24.72**	*12.63*	**3.74**	*2.36*
MIS 8	2320.0	2398.6	-444.5	-421.5	**76.76**	*35.00*	**112.06**	*38.05*	**26.24**	*17.20*	**3.84**	*5.24*
MIS 10	2599.9	2650.0	-445.0	-425.1	**77.80**	*32.30*	**112.76**	*61.56*	**30.21**	*19.92*	**5.77**	*9.76*
MIS 12	2783.2	2794.9	-440.9	-422.5	**72.70**	*19.82*	**138.46**	*34.04*	**48.69**	*22.43*	**3.93**	*3.32*
MIS 14.2	2915.7	2919.9	-436.4	-429.3	**70.88**	*15.13*	**110.46**	*21.66*	**34.33**	*17.31*	**3.16**	*5.70*
MIS 16	3037.6	3039.8	-441.0	-412.3	**78.23**	*12.32*	**111.67**	*21.46*	**32.89**	*11.94*	**3.07**	*4.96*
MIS 18	3137.8	3153.1	-441.4	-423.7	**80.44**	*13.94*	**114.44**	*31.38*	**26.28**	*13.95*	**3.26**	*3.98*
Clean Facies	3201.0	3248.0	-442.5	-427.7	**71.78**	*3.79*	**99.91**	*13.39*	**29.03**	*2.42*	**1.94**	*2.40*
Dispersed Facies	3248.0	3259.3	-443.2	-436.7	**93.16**	*15.43*	**141.68**	*30.42*	**46.26**	*15.37*	**2.68**	*4.17*

Table 1: Mean concentration and 1σ values (ngg^{-1} or ppb) for selected chemical species in the Clean and Dispersed Basal ice facies of the EPICA Dome C ice core, as compared to those of the previous full glacial periods (see text for details). Depth (meters) and δD (‰) ranges are given for each time interval considered.

Formatted: Right: 2.54 c cm, Width: 27.94 cm, Heig cm

Figure Captions

Figure 1: a) visual appearance of the EDC basal ice in the lower meters of the core (photo: D. Dahl-Jensen), b) EDC δD_{ice} vs. depth, c) EDC δD_{ice} vs. age (EDC3 time scale extended to the basal ice layers), d) Combined Vostok and EDC $\delta^{18}O_{atm}$ vs. age (adapted from Dreyfus et al., 2007), e) $\delta^{18}O$ vs. age for the benthic record stack of Lisiecki and Raymo (2005), and f) Integrated summer insolation for various thresholds (τ) at 30°N vs. age, as calculated by Huybers (2006). For reasons described in the text, ice below 3189.45m depth is referred to as « clean ice facies » (blue squares) and « dispersed ice facies » (red triangles) describes the ice below 3248.30m, where solid inclusions are visible.

Figure 2: a) δD_{ice} (‰) vs. $\delta^{18}O_{ice}$ (‰) and b) d (deuterium excess ‰) vs. δD_{ice} (‰) for the clean (open squares) and dispersed (open triangles) basal ice facies at EPICA Dome C, as compared to the ice from the 0-140 ky interval (black dots, Stenni et al., 2010). See text for details.

Figure 3: Gas and dust properties of the clean (squares) and dispersed (triangles) basal ice facies at EPICA Dome C: a) total gas content ($ml_{air}g_{ice}^{-1}$, dark grey), methane (ppbV, white), nitrous oxide (ppbV, light grey) and carbon dioxide (ppmV, black) - vertical bars of equivalent shading cover the full concentrations range observed for CH_4, CO_2, N_2O and total gas content during the preceding climatic cycles, b) dust concentrations (ppb) -black vertical bar covers the full concentration range during the previous climatic cycles.

Figure 4: Concentrations (in ppb or ngg^{-1}) of selected chemical species in the clean (open squares) and dispersed (open triangles) basal ice facies of the EPICA Dome C core, as compared to those of the preceding climatic cycles (black dots, courtesy of the EPICA chemical consortium). Resolution is between 5 and 8 cm above 3200m depth and between 1.5 and 5 cm in the basal ice below 3200 m. Note the change of depth scale below 3200m.

Figure 5: Frequency distribution of concentrations (in bins of 1 or 5 ngg^{-1} or ppb) of selected chemical species in the clean (open squares - thick black solid line) and dispersed (open triangles - thick black dotted line) basal ice facies of the EPICA Dome C core, as compared to those for the preceding full glacial periods (incremented symbols and thin grey lines - courtesy of EPICA Chemistry Consortium). See text for definition of « full glacials ».

Figure 6: Mean equivalent crystals radii in the basal ice layers of the EPICA Dome C ice core, as compared to measurements in ice above 3200m depth from Durand et al. (2007). Basal ice measurements are preliminary results obtained using the linear intercept technique « on site», while the data from above 3200m were obtained using Automatic Ice Texture Analyzers (AITAs - Wang and Azuma, 1999; Russell-Head and Wilson, 2001; Wilen et al., 2003).

Figure 7: Schematic illustration of the hypothesized impact of the confining bedrock topography (bedrock valleys about 20 km wide and 200-400 meters deep - from Remy and Tabacco, 2000) on the stress regime, layer thickness and ice fabric patterns in the bottom ice of EPICA Dome C. Vertical stretching is accommodated by basal melting and/or along sub-glacial valley flow. For

clarity, this illustration enhances the process so that absolute annual layer thickness increases downwards. A milder effect would only result in a decrease of the thinning rate (see text for details).

Figure 8: Sketch of potential chemical sorting effects during enhanced migration recrystallization processes under a changing stress field, close to the pressure melting point, in the clean and dispersed basal ice facies of EPICA Dome C. Processes in italic/dotted arrows are hypothetical (see text for details).

Figure 9: Attempting to reconstruct the time scale for the basal ice sequence: a) Zoom on the $\delta^{18}O_{atm}$ curve vs. Integrated summer insolation at 30°N (see Fig. 1e) and b) Comparison of the benthic $\delta^{18}O$ curve (open circles) to the EPICA δDice profile (black dots), where the basal ice time scale was linearly « compressed » using tie points 1 and 2 in a) (see text for details)

Figure S1: Plot of the mean (a) and 1σ (b) values for the various chemical elements measured in each of the glacial periods considered in this study and for the Clean (open squares) and Dispersed (open triangles) basal ice samples as a function of the duration (in thousand years) of the « full glacial period » selected on the basis of the δD-values. Isotopic Stage 18, which is already thought to show increased variability for some of the elements, is shown as an open star. Duration is estimated from the EDC-3 time scale (Parrenin, 2007).

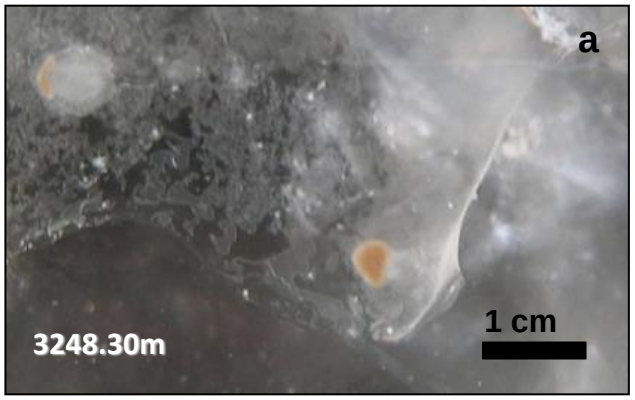
a
3248.30m
1 cm

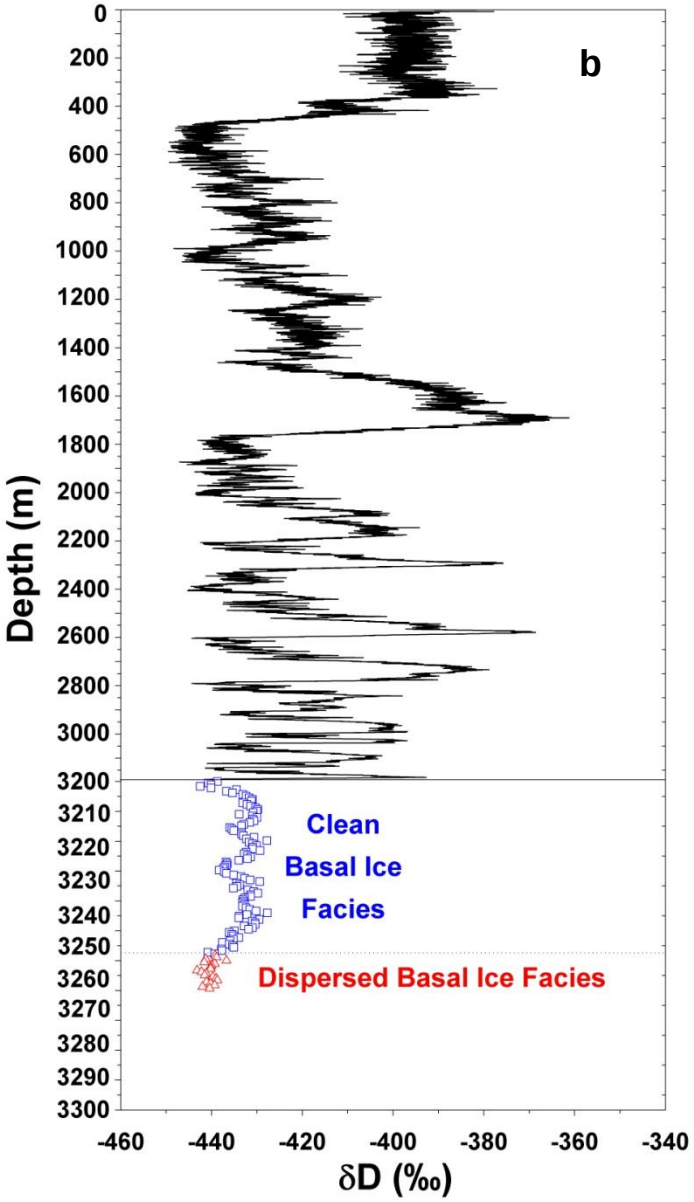
b
Depth (m)
δD (‰)
Clean
Basal Ice
Facies
Dispersed Basal Ice Facies

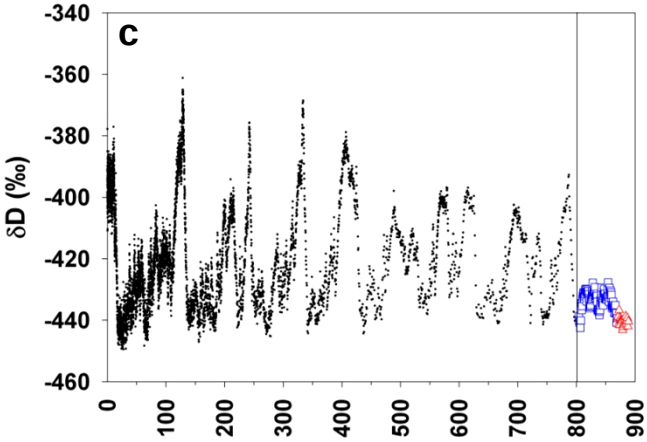
c
δD (‰)

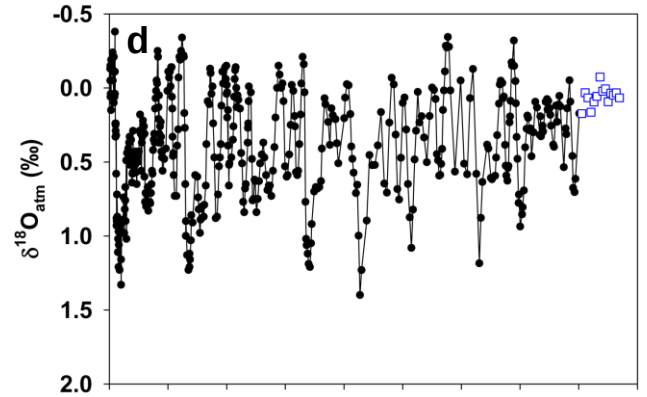
d
δ18Oatm (‰)

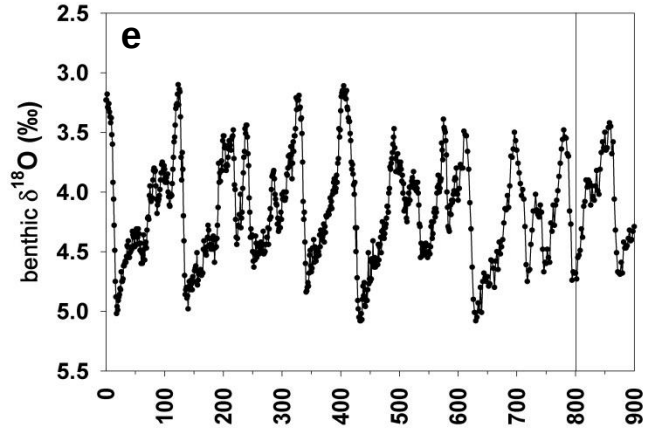
e
benthic δ18O (‰)

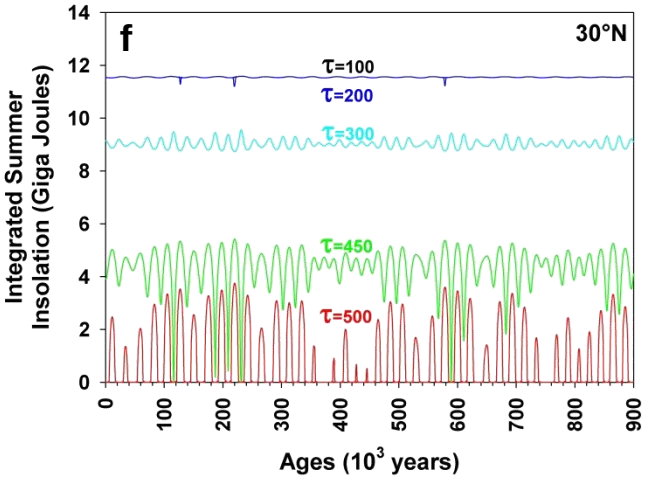
f
30°N
τ=100
τ=200
τ=300
τ=450
τ=500
Integrated Summer Insolation (Giga Joules)
Ages (10³ years)

Figure 1

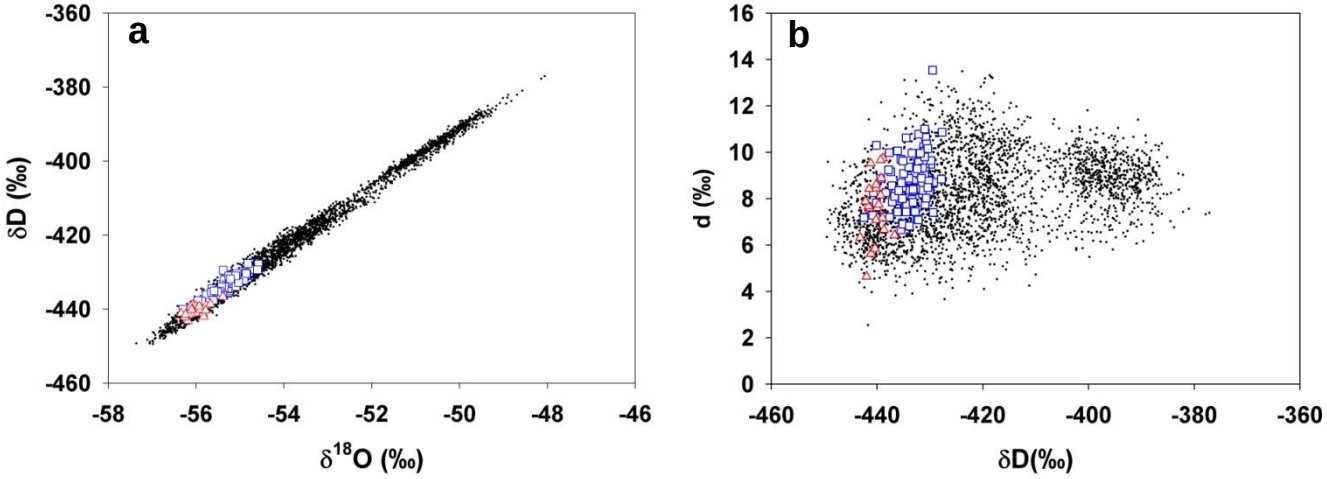
a
-360
-380
-400
-420
-440
-460
δD (‰)
-58
-56
-54
-52
-50
-48
-46
δ18O (‰)
b
16
14
12
10
8
6
4
2
0
d (‰)
-460
-440
-420
-400
-380
-360
δD(‰)

Figure 2

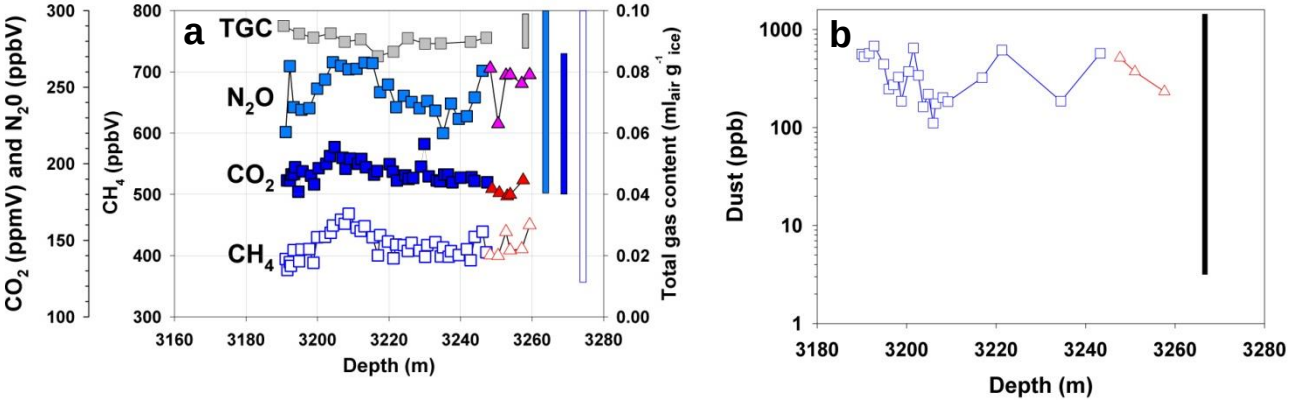
a
TGC
N_2O
CO_2
CH_4
CO_2 (ppmV) and N_2O (ppbV)
CH_4 (ppbV)
Total gas content (ml_{air} g^{-1}_{ice})
Depth (m)
b
Dust (ppb)
Depth (m)

Figure 3

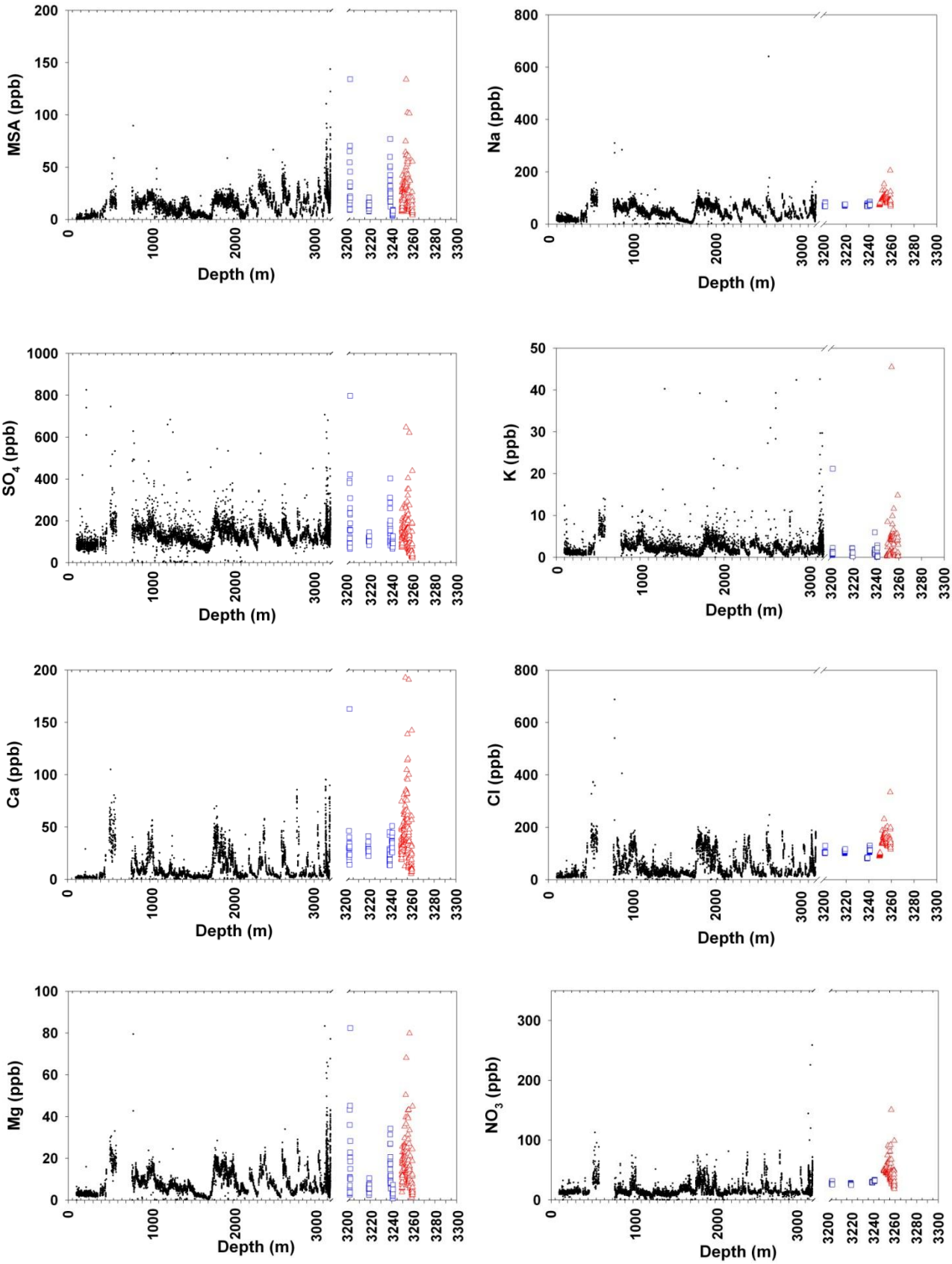

Figure 4

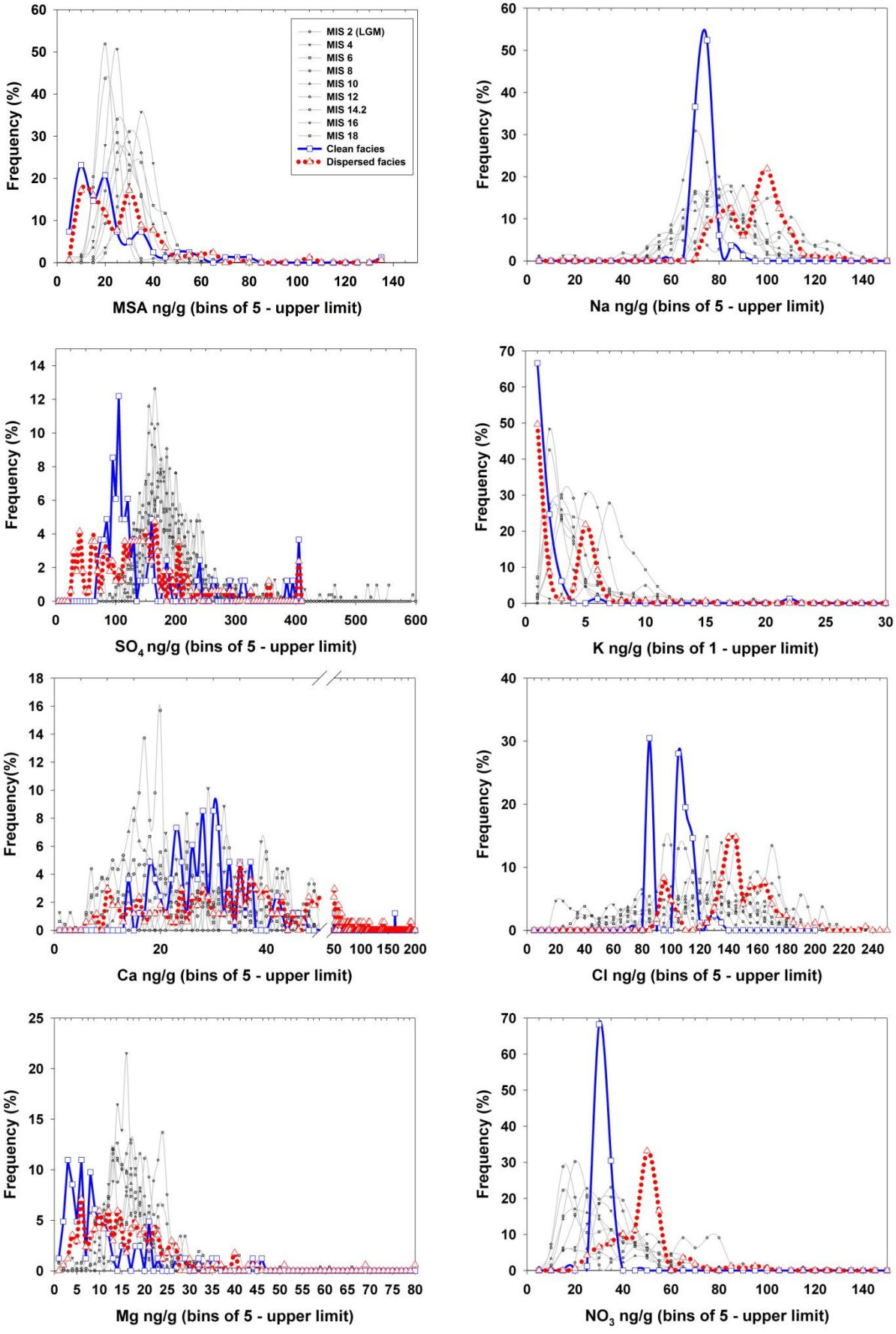
MIS 2 (LGM)
MIS 4
MIS 6
MIS 8
MIS 10
MIS 12
MIS 14.2
MIS 16
MIS 18
Clean facies
Dispersed facies
Frequency (%)
MSA ng/g (bins of 5 - upper limit)
Na ng/g (bins of 5 - upper limit)
SO4 ng/g (bins of 5 - upper limit)
K ng/g (bins of 1 - upper limit)
Frequency(%)
Ca ng/g (bins of 5 - upper limit)
Cl ng/g (bins of 5 - upper limit)
Mg ng/g (bins of 5 - upper limit)
NO3 ng/g (bins of 5 - upper limit)

Figure 5

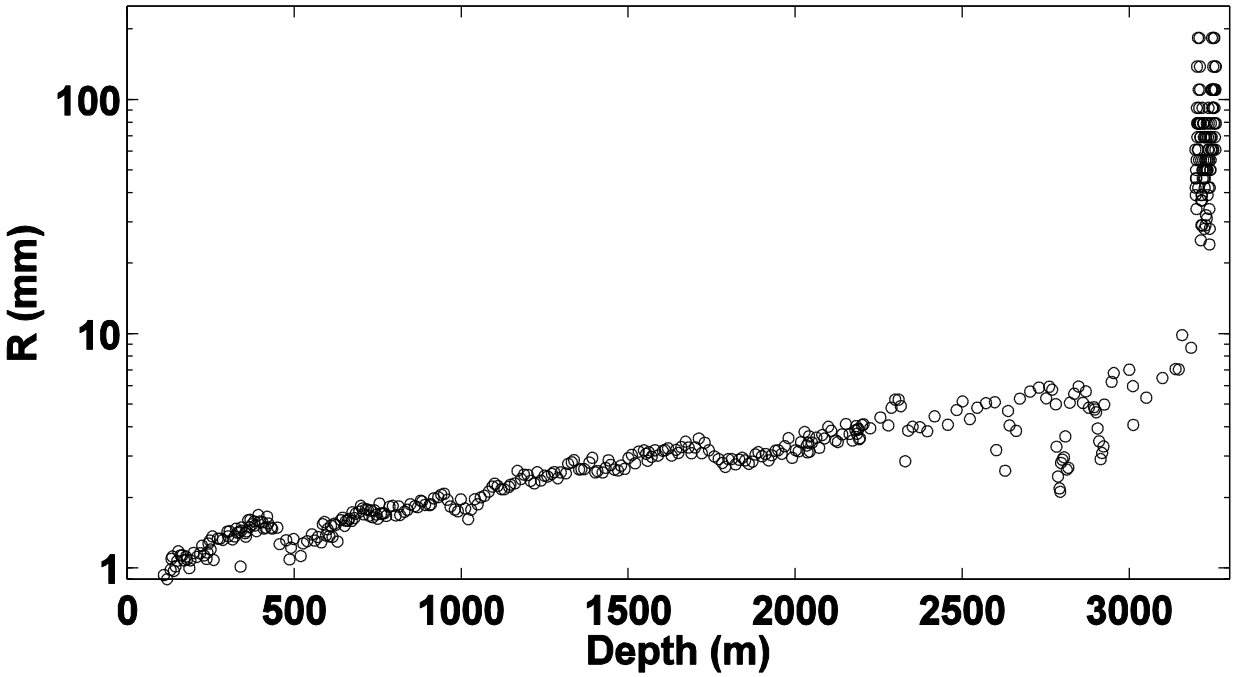

Figure 6

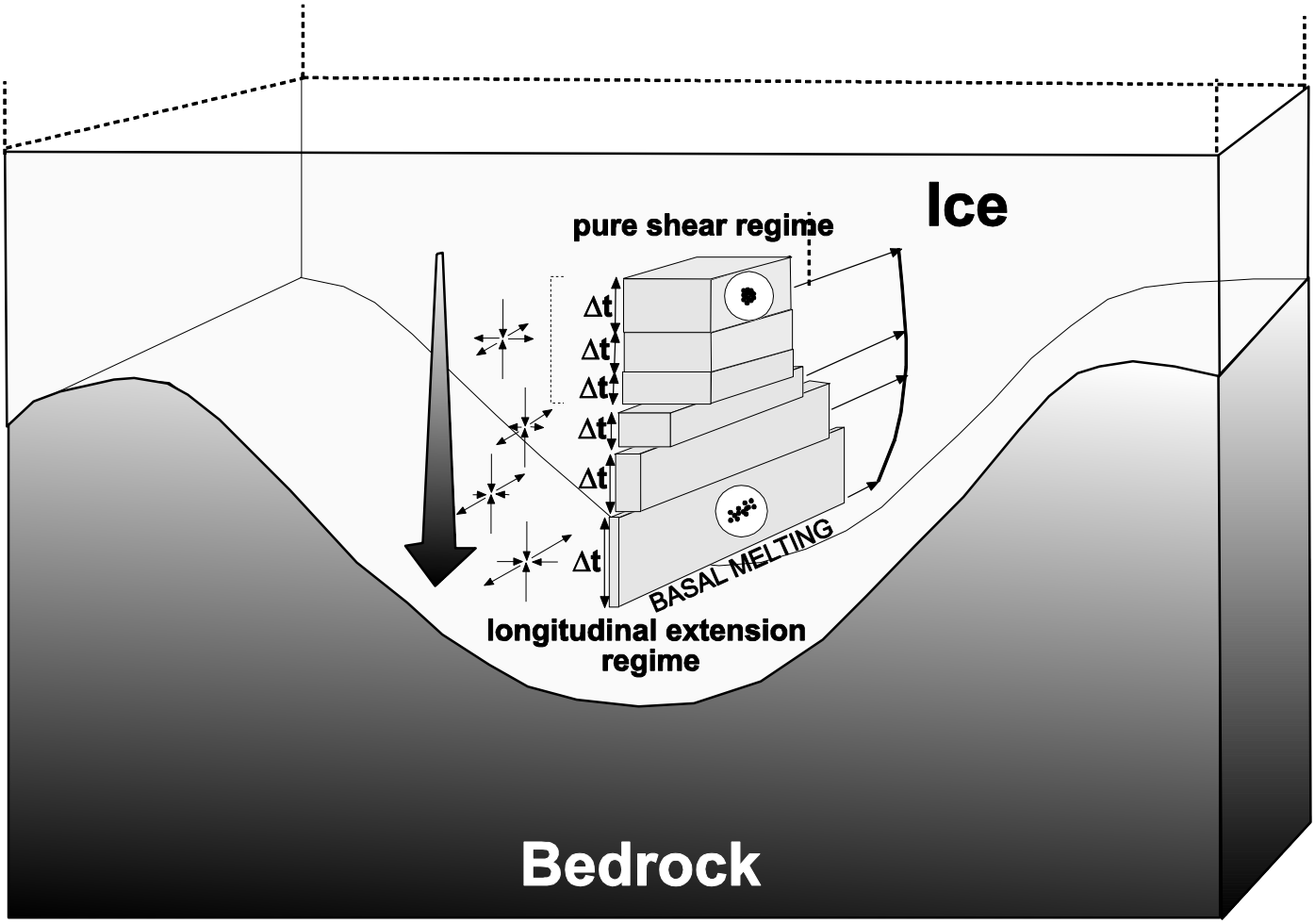
Ice
pure shear regime
Δt
Δt
Δt
Δt
Δt
Δt
BASAL MELTING
longitudinal extension
regime
Bedrock

Figure 7

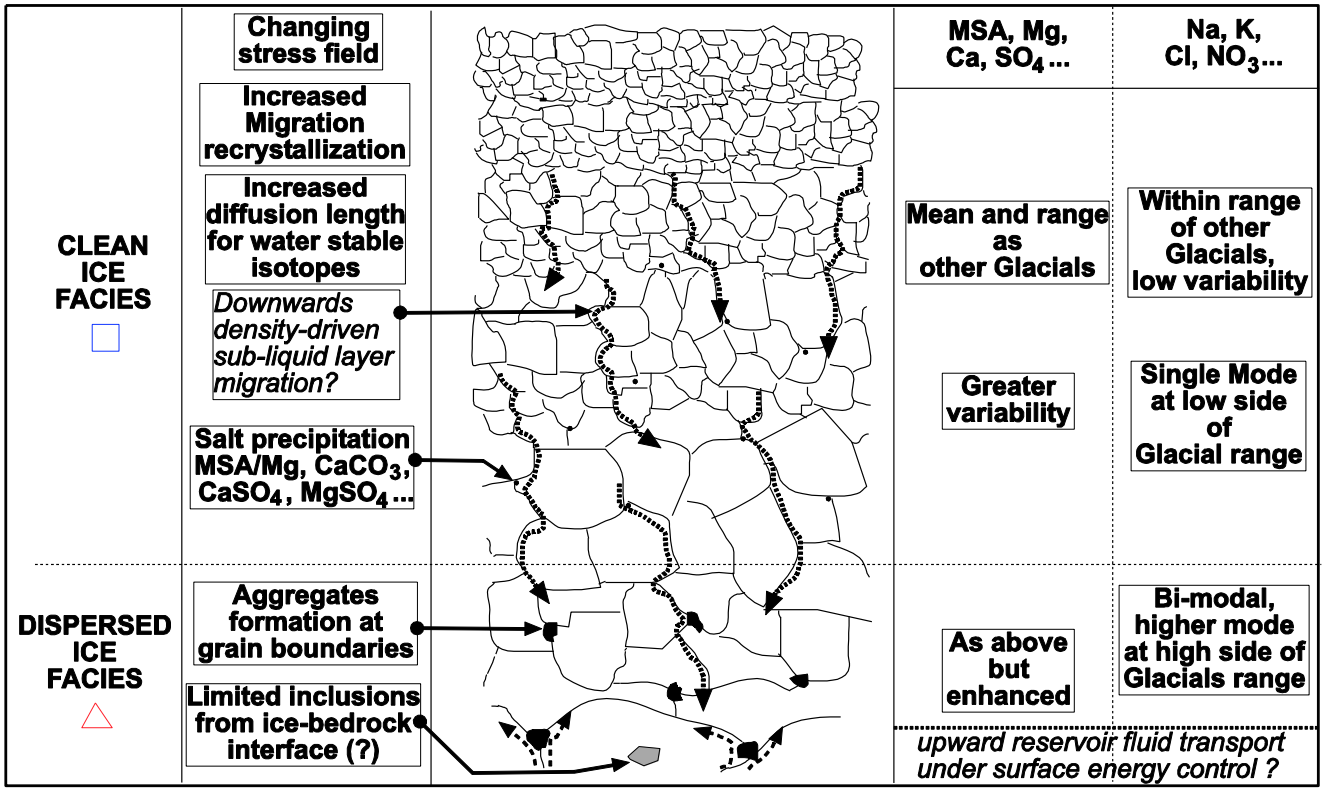
Changing stress field
Increased Migration recrystallization
Increased diffusion length for water stable isotopes
Downwards density-driven sub-liquid layer migration?
Salt precipitation MSA/Mg, $CaCO_3$, $CaSO_4$, $MgSO_4$...
Aggregates formation at grain boundaries
Limited inclusions from ice-bedrock interface (?)
MSA, Mg, Ca, SO_4...
Na, K, Cl, NO_3...
CLEAN ICE FACIES
Mean and range as other Glacials
Within range of other Glacials, low variability
Greater variability
Single Mode at low side of Glacial range
DISPERSED ICE FACIES
As above but enhanced
Bi-modal, higher mode at high side of Glacials range
upward reservoir fluid transport under surface energy control ?

Figure 8

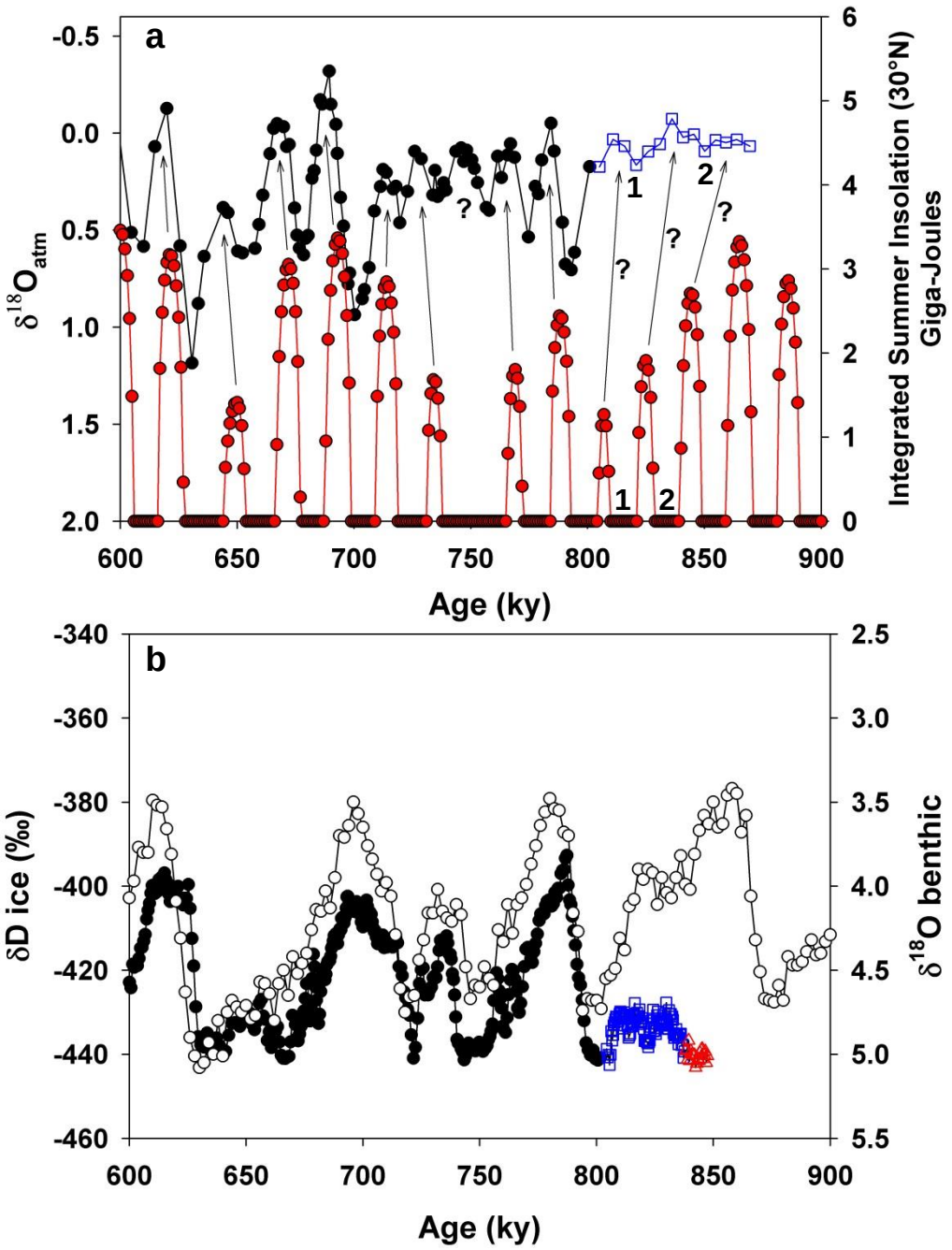
a
-0.5
0.0
0.5
1.0
1.5
2.0
δ18Oatm
6
5
4
3
2
1
0
Integrated Summer Insolation (30°N)
Giga-Joules
1
2
?
?
?
?
1
2
600
650
700
750
800
850
900
Age (ky)
b
-340
-360
-380
-400
-420
-440
-460
δD ice (‰)
2.5
3.0
3.5
4.0
4.5
5.0
5.5
δ18O benthic
600
650
700
750
800
850
900
Age (ky)

Figure 9